Quantitative Proteomic Profiling of Prostate Cancer Reveals a Role for miR-128 in Prostate Cancer*[S]

Amjad P. Khan,[a,b,c] Laila M. Poisson,[c,d] Vadiraja B. Bhat,[e,f] Damian Fermin,[b] Rong Zhao,[a,b] Shanker Kalyana-Sundaram,[a,b] George Michailidis,[g] Alexey I. Nesvizhskii,[b,h] Gilbert S. Omenn,[h,i,j] Arul M. Chinnaiyan,[a,b,h,j,k,l] and Arun Sreekumar[a,b,j,m]

Multiple, complex molecular events characterize cancer development and progression. Deciphering the molecular networks that distinguish organ-confined disease from metastatic disease may lead to the identification of biomarkers of cancer invasion and disease aggressiveness. Although alterations in gene expression have been extensively quantified during neoplastic progression, complementary analyses of proteomic changes have been limited. Here we interrogate the proteomic alterations in a cohort of 15 prostate-derived tissues that included five each from adjacent benign prostate, clinically localized prostate cancer, and metastatic disease from distant sites. The experimental strategy couples isobaric tags for relative and absolute quantitation with multidimensional liquid phase peptide fractionation followed by tandem mass spectrometry. Over 1000 proteins were quantified across the specimens and delineated into clinically localized and metastatic prostate cancer-specific signatures. Included in these class-specific profiles were both proteins that were known to be dysregulated during prostate cancer progression and new ones defined by this study. Enrichment analysis of the prostate cancer-specific proteomic signature, to gain insight into the functional consequences of these alterations, revealed involvement of miR-128-a/b regulation during prostate cancer progression. This finding was validated using real time PCR analysis for microRNA transcript levels in an independent set of 15 clinical specimens. miR-128 levels were elevated in benign prostate epithelial cell lines compared with invasive prostate cancer cells. Knockdown of miR-128 induced invasion in benign prostate epithelial cells, whereas its overexpression attenuated invasion in prostate cancer cells. Taken together, our profiles of the proteomic alterations of prostate cancer progression revealed miR-128 as a potentially important negative regulator of prostate cancer cell invasion. ***Molecular & Cellular Proteomics 9:298–312, 2010.***

Prostate cancer is the second most common cause of cancer-related death in America and afflicts one of nine men over the age of 65. The American Cancer Society estimates that 186,320 American men will be diagnosed with prostate cancer and 28,660 will die this year (1). The advent of prostate-specific antigen (PSA)[1] screening has led to earlier detection of prostate cancer (2). Coincident with increased serum PSA testing, there has been a dramatic increase in the number of prostate needle biopsies performed (3). This has resulted in a surge of equivocal prostate needle biopsies (4) and men with the looming threat of prostate cancer. However, the stage shift associated with the advent of PSA screening may also be associated with diagnosis of a substantial number of prostate cancer cases that may have non-aggressive clinical natural history or so-called "indolent" prostate cancers (5, 6). Even before the advent of PSA screening, it was noted that up to 70–80% of Gleason score 6 cancers and as many as 20% of Gleason score 7 cancers may have a non-aggressive course without cancer death if observed without intervention for more than 15 years (7). With the population of males 65 years and older expected to increase from 14 million in year 2000 to 31 million by 2030 (8), it will be increasingly important to discern such indolent prostate cancer from aggressive cancers that warrant intervention.

From [a]The Michigan Center for Translational Pathology, [k]Howard Hughes Medical Institute, [h]Center for Computational Medicine and Biology, Departments of [b]Pathology, [d]Biostatistics, [g]Statistics, and [i]Internal Medicine, and the [j]Comprehensive Cancer Center, University of Michigan Medical School, Ann Arbor, Michigan 48109 and [e]Department of Pathology, Scott and White Hospital, Temple, Texas 76508

Received, March 24, 2009, and in revised form, October 21, 2009
Published, MCP Papers in Press, November 9, 2009, DOI 10.1074/mcp.M900159-MCP200

[1] The abbreviations used are: PSA, prostate-specific antigen; BPH, benign prostatic hyperplasia; PCA, prostate cancer; OCM, Oncomine Concepts Map; Benign, benign adjacent prostate; Mets, metastatic prostate tumor; iTRAQ, isobaric tags for relative and absolute quantitation; Q-PCR, quantitative RT-PCR; PHB, Prohibitin; SCX, strong cation exchange; IPI, International Protein Index; FDR, false discovery rate; ID, identification; PrEC, prostate epithelial cells; GOLM1, Golgi membrane protein 1; TMSB10, Thymosin β10; VIM, Vimentin; APRIL, A Proliferation Inducing Ligand; VCP, Valosin Containing Protein; LPP, Lipoma Preferred Partner; TROVE, Telomerase R_O and Vault; C_T, threshold cycle.

© 2010 by The American Society for Biochemistry and Molecular Biology, Inc.
This paper is available on line at http://www.mcponline.org

ASBMB MOLECULAR & CELLULAR PROTEOMICS MCP

ASBMB MOLECULAR & CELLULAR PROTEOMICS MCP

Prostate cancer, like other cancers, develops in the background of diverse genetic and environmental factors (9). Multiple, complex molecular events characterize prostate cancer initiation, unregulated growth, invasion, and metastasis. Distinct sets of genes, proteins, and metabolites dictate progression from precursor lesion, to localized disease, and finally to metastatic disease. Clinically localized prostate cancer can be effectively ablated using surgical or radiation treatments. Androgen ablation is the most common therapy for advanced prostate cancer, leading to massive apoptosis of androgen-dependent malignant cells and temporary tumor regression. In most cases, however, the tumor re-emerges, can proliferate independently of androgen or antiandrogen signals, and develops into a metastatic disease that is invariably incurable. With the advent of global profiling strategies, a systematic analysis of molecular alterations involved in prostate cancer is now possible.

Importantly, deciphering the molecular networks that distinguish progressive disease from non-progressive disease will shine light on the biology of aggressive prostate cancer as well as lead to the identification of biomarkers that will aid in the selection of patients who should be treated (10). To begin to understand prostate cancer progression with a systems perspective, we need to characterize and integrate the molecular components involved (11–14). A number of groups have used gene expression microarrays to profile prostate cancer tissues (15–23) as well as other tumors (24–27) at the transcriptome level, but much less work has been done at the protein level.

Proteins, as opposed to nucleic acids, represent the functional effectors of cancer progression and thus serve as therapeutic targets as well as markers of disease. Proteomics approaches will facilitate the identification of proteins and biochemical pathways involved in tumor development. Proteomics studies will also facilitate identification of differential post-translational modifications that play a major role in cellular functions. Nelson *et al.* (28) carried out protein expression profiles of androgen-stimulated prostate cancer cells using two-dimensional electrophoresis. Ahram *et al.* (29) identified cellular proteomes of matched normal prostate epithelial cells and high grade prostate cancer cells using a combination of tissue microdissection, two-dimensional electrophoresis, and mass spectrometry. Multiple technologies have been used to identify proteomic alterations in the serum of prostate cancer patients including protein microarray and SELDI (13, 30). However, studies quantifying proteomic alterations in tumor specimens in an unbiased manner have been limited (31–35). Recently Garbis *et al.* (32) and Ralhan *et al.* (35) have used iTRAQ-based quantification to assess global alterations in the proteome using tissues from prostate cancer and head and neck cancer patients, respectively. We used a similar approach to quantify global changes associated with the prostate cancer proteome in the stages of progression from organ-confined to metastatic disease. Additionally, we extended our analysis beyond delineation of tumor-specific proteomic signatures to nominate and confirm the miR-128 pathway as a critical intermediary in tumor invasion.

EXPERIMENTAL PROCEDURES

Patient Population and Sample Selection

The Institutional Review Board of the University of Michigan Medical School approved this study on discovery of proteomic alterations of prostate cancer progression. Tissue samples obtained postsurgery from clinically localized prostate cancer patients (PCA; $n = 5$), advanced prostate cancer patients (Mets; $n = 5$), and benign adjacent controls (Benign; $n = 5$) were procured in a frozen state from the University of Michigan Specialized Research Program in Prostate Cancer (Specialized Program of Research Excellence) tissue bank. Two men provided both tumor and benign tissue samples. All other tissue samples were from unique patients. Deidentified numeric specimen codes were used to protect the identity of the men. Detailed clinical and pathology data for this study are available in supplemental Table 1. The histological diagnosis of each sample was confirmed by microscopic examination of hematoxylin- and eosin-stained frozen sections by a board-certified pathologist.

Chemicals and Reagents

All chemicals were purchased from Sigma unless otherwise mentioned.

Antibodies

Mouse monoclonal antibodies directed to Vimentin (VIM), Ezrin, RAN, and fatty-acid synthase and polyclonal antibodies to SLC25A3, Thymosin β10 (TMSB10), and Prohibitin (PHB) were purchased from BD Biosciences and Novus Biologicals (Littleton, CO), respectively. Goat polyclonal antibodies against ARF1, APRIL (ANP32B), and glyceraldehyde-3-phosphate dehydrogenase were procured from Abcam Inc. (Cambridge, MA), and VCP antibodies were purchased from Santa Cruz Biotechnology (Santa Cruz, CA). Antibodies to RAP1B and TROVE domain family member 2 (TROVE2) were purchased from Cell Signaling Technologies (Danvers, MA) and Genway (San Diego, CA), respectively. Rabbit polyclonal antibodies to Golgi membrane protein 1 (GOLM1) were a kind gift from Dr. Claus J. Fimmel (Edward Hines Veterans Affairs Medical Center, Hines, IL).

Protein Extraction

For protein extraction, the tissue samples were resuspended in lysis buffer consisting of 7 M urea, 2 M thiourea, 100 mM DTT, 0.5% Bio-Lyte pH 3–10 (Bio-Rad), 2% octyl glucoside, and 1 mM PMSF. Samples were lysed at room temperature for 30 min followed by centrifugation at 35,000 rpm at 4 °C for 1 h. The protein solution was exchanged into 50 mM triethylammonium bicarbonate, pH 9 using a PD-10 column according to the manufacturer's instruction (GE Healthcare). Total protein content was measured using the Bradford assay (Bio-Rad), and the lysates were stored at −80 °C for future use.

Protein Digestion and iTRAQ Labeling

200 μg of total protein from each tissue sample were used to generate iTRAQ-labeled peptides according to the manufacturer's protocol. Specifically, the proteins were first subjected to reduction and alkylation using DTT and iodoacetamide provided in the iTRAQ labeling kit (iTRAQ® Reagents Multiplex kit, Applied Biosystems, Foster City, CA). They were then digested to peptides using porcine trypsin (1:50; Promega, Madison, WI) in 50 mM triethylammonium bicarbonate, pH 9. The digestion was performed for 24 h at 37 °C. At

the end of 24 h, the trypsin activity was stopped using 3% formic acid. The digested peptides were subjected to iTRAQ labeling according to the protocol described previously (36). The iTRAQ experiments were performed in five sets, each containing four samples. Specifically, for labeling, 100 μg of protein each from Benign, PCA, and Mets were labeled with isobaric tags 114, 115, and 116, respectively (Fig. 1). A reference pool containing 67 μg of protein from each of the tissue samples ($n = 5$ each of Benign, PCA, and Mets) used in the study was created (total protein amount in the pool, 1 mg) and labeled with isobaric tag 117 (see Fig. 1). 50 μg of peptides labeled with each of the four isobaric labels were combined and subjected to two-dimensional fractionation coupled to tandem mass spectrometry (Fig. 1).

SCX Fractionation

200 μg of iTRAQ-labeled peptide samples described above were completely dried in a SpeedVac, resuspended in 40 μl of 0.1% formic acid in 5% acetonitrile (mobile phase A), and directly loaded onto a 1 × 150-mm polysulfoethyl aspartamide strong cation exchange column (Michrom Bioresources, Auburn, CA) using an Agilent 1200 auto sampler. Buffer containing 1 M ammonium formate, 10% formic acid in 5% acetonitrile (mobile phase B) was used to create a linear chromatographic gradient at a flow rate of 50 μl/min. A total of 10 fractions were collected over a 40-min gradient encompassing a salt concentration of 0–100 mM ammonium formate. An additional five fractions were generated over the next 10 min at a higher salt concentration range of 100–1000 mM. Fractionated peptides were completely dried and reconstituted in 10 μl of 0.1% TFA prior to LC-MS/MS analysis.

HPLC-Chip/Mass Spectrometry Analysis

Refer to Fig. 1 for an outline. A total of 3 μl of reconstituted peptide mixture (~30% of SCX fraction) was injected onto an LC-MS system consisting of a 1200 Series liquid chromatograph, HPLC-Chip Cube MS interface, and 6510 Q-TOF mass spectrometer (all Agilent Technologies, Santa Clara, CA). The system was equipped with an HPLC-Chip (Agilent Technologies) that incorporated either a 40-nl enrichment column and a 43 mm × 5 μm reverse phase column (*low capacity chip*) or a 160-nl enrichment column and a 150 mm × 75 μm reverse phase column (*high capacity chip*). In both cases, the reverse phase column was packed with Zorbax 300SB-C18 5-μm particles. Three analytical replicates of each of the five iTRAQ sets were analyzed by mass spectrometry. This included duplicate analysis on the high capacity chip (henceforth termed high capacity 1 and high capacity 2) and a single run on a low capacity chip (henceforth termed low capacity). Overall the experimental design resulted in a total of 15 independent mass spectrometry data points or experiments ($n = 3$ for each iTRAQ set) for the entire study.

For each mass spectrometry experiment, peptides were loaded onto the enrichment column with 97% solvent A (water with 0.1% formic acid). A two-step gradient generated at a flow rate 0.3 μl/min was used for peptide elution. This included a linear gradient from 3% B (acetonitrile with 0.1% formic acid) to 45% B over 25 min followed by a sharp increase to 90% B within 5 min. The total run time, including column reconditioning, was 40 min. The column effluent in all cases was directly analyzed by the 6510 Q-TOF mass spectrometer that was interfaced in tandem through an HPLC-Chip Cube nanospray source. The latter was operated at a capillary voltage of 1900 V with a capillary current of 1.1 μA in 1 GHz. The MS data were acquired in the positive ionization mode using Agilent MassHunter Workstation Q-TOF B.01.03. During the course of data acquisition, the fragmentor voltage, skimmer voltage, and octopole RF were set to 175, 65, and 750 V, respectively. Auto-MS/MS was performed with a total cycle time of 1.97 s. In each cycle, MS spectra were acquired at 3 Hz (three spectra/s) (*m/z* 450–1500), and the four most abundant ions (with charge states 2+, 3+, and >3+) exceeding 2000 counts were selected for MS/MS at 3 Hz (three spectra/s) (*m/z* 50–2000). A medium isolation (4 *m/z*) window was used for precursor isolation. A collision energy with slope of 3.9 V/100 Da and offset of 2.9 V was used for fragmentation. Reference mass correction was activated using a reference mass of 1221.99. Precursors were set in an exclusion list for 0.5 min after two MS/MS spectra.

Mass Spectral Data Analysis

MS/MS spectra generated above were extracted from the raw data in mzXML file format using a converter from the Institute for Systems Biology (trapper). The mzXML files were searched using SEQUEST against the human International Protein Index (IPI) database version 3.26 (containing 67,655 entries) appended with an equal number of decoy sequences (reversed sequences from the original database). The following search parameters were selected: 0.5-Da precursor mass tolerance, monoisotopic mass, semitryptic search with two or fewer missed cleavages, oxidized methionine specified as a variable modification, and iTRAQ label on Lys and at the peptide N terminus as fixed modifications. In total, 1,155,545 SEQUEST search results (mostly from doubly and triply charged spectra) were obtained. The search results were further processed using the Trans-Proteomic Pipeline (TPP), which includes the PeptideProphet and ProteinProphet tools for peptide and protein level analysis and LIBRA for peptide quantification using iTRAQ signature ions (37). Default settings were used for each of these programs. A weighted average of the peptide intensities per protein was used to quantify the protein. Proteins were referenced by IPI number. Gene symbol information for the IPI numbers was taken from the EMBL-EBI database for human IPI numbers on March 7, 2008.

As the next step, data from the 15 mass spectrometry measurements were merged into a single file. To align proteins with their most likely counterparts across the experiments (supplemental Fig. S1) the 15 individual PeptideProphet files were run together through ProteinProphet, and the combined protein file was generated (master protein identification list). In-house written software was then applied to extract, for each protein group in the master list, information from the individual ProteinProphet files (probability, number of spectra, and quantitative information). For each protein group in the master file, the IPI accession with the most evidence across the 15 iTRAQ experiments (*i.e.* reported in the most XML files) was retained. Then, the maximum probability score (Pw), provided by Protein Prophet, across the 15 iTRAQ experiments was calculated and taken as the primary score for filtering the data. We chose to threshold the data, retaining only proteins (*i.e.* IPI accessions) whose maximum protein probability was at least 0.955. This threshold amounted to an estimated false discovery rate (FDR) of 2%, calculated as the number of reverse proteins identified divided by the number of forward proteins identified (37) (supplemental Fig. S2). We further limited the data by removing all proteins with a single peptide identification resulting in an estimated FDR of 1.4%.

Statistical Analysis

For the purpose of this analysis, we are interested in comparing protein expression between local tumor and benign tissues (PCA *versus* Benign, ratio 115/114) and between metastatic tumor and local tumor tissues (Mets *versus* PCA, ratio 116/115). These relative quantities are used on a log scale (base 2). Given the three MS runs or scanners (high capacity 1 and 2 and low capacity; see above for details) used to evaluate the samples (each quadruplex iTRAQ), each protein (*i.e.* IPI accession) can be measured up to three times per

ASBMB MOLECULAR & CELLULAR PROTEOMICS MCP

sample. For analysis, we combine these replicate measures using a weighted average where the inverse sample variance is the weight. Specifically, let the mass spectrometer assessments be labeled *A*, *B*, and *C*. For each sample *i* and protein *j*, we calculate the weighted average y_{ij} by Equation 1. Note that only measured samples contribute to this weighted average. If, say, a protein *k* was measured by only scanner *A* for sample *i*, then $y_{ik} = x_{Aik}$ as in Equation 2.

$$y_{ij} = \frac{\sum_{d \epsilon A,B,C} \frac{x_{dij}}{\mathrm{var}(x_{di})}}{\sum_{d \epsilon A,B,C} \frac{1}{\mathrm{var}(x_{di})}} = \frac{\frac{x_{Aij}}{\mathrm{var}(x_{Ai})} + \frac{x_{Bij}}{\mathrm{var}(x_{Bi})} + \frac{x_{Cij}}{\mathrm{var}(x_{Ci})}}{\frac{1}{\mathrm{var}(x_{Ai})} + \frac{1}{\mathrm{var}(x_{Bi})} + \frac{1}{\mathrm{var}(x_{Ci})}} \quad \text{(Eq. 1)}$$

$$y_{ij} = \frac{\frac{x_{Aij}}{\mathrm{var}(x_{Ai})}}{\frac{1}{\mathrm{var}(x_{Ai})}} = x_{Aij} \quad \text{(Eq. 2)}$$

Given that the same set of proteins was not measured in each ITRAQ experiment and that the quantification is relative, we chose to analyze each of the five ITRAQ experiments separately. Specifically, we assume that each experiment is composed of a mixture of three distributions: 10% up-regulated, 10% down-regulated, and 80% unchanged. We assume that on the $\log_2$ scale the unchanged measurements form a symmetric distribution and thus trim the upper 10% and lower 10% of the data points to arrive at a trimmed distribution representing the null or unchanged measurements. We chose the threshold for dysregulation as the mean of the trimmed data ± 1.5 times the standard deviation of the trimmed data. To reduce spurious results, for localized tumor tissue compared with benign adjacent tissue, we required that the protein be detected in at least two samples and that at least two of these samples showed dysregulation in the same direction to be considered further. Proteins with discordant expression patterns within samples of a given diagnostic class were not considered among those dysregulated.

For metastatic tumors *versus* localized tumors, we expected to see more dysregulation so we assumed 20% of the proteins were up-regulated, 20% were down-regulated, and 60% were unchanged. Again, the sample trimmed mean and trimmed standard deviation were used to construct the thresholds. However, as we expect more spurious results due to differences in the site of metastasis, we require the protein to be detected in at least three samples and have concordant results in at least 60% of the samples detected for further consideration.

Heat Map Plots

Heat maps were drawn using the image function in R (38). The color coding is derived using the ranking of the log ratio in the distribution of measures for that sample. Shades of green represent down-regulation, and shades of red represent up-regulation. The intensity of the color is determined by the distance (in standard deviations) from the mean of the trimmed distribution.

Oncomine Concept Map Analyses

Mapping of Proteomics Data to Common Identifier—Protein identifications (IPI numbers) belonging to PCA-specific or Mets-specific signatures were converted to Human Genome Organisation gene symbols and batch-loaded to Oncomine Concepts Map (OCM) for analysis as described below. The conversion to gene symbol requires that potential isoforms, *i.e.* multiple IPI numbers associated with a single gene symbol, contribute only once in the enrichment analysis.

Enrichment of Molecular Concepts—To explore the network of inter-relationships among various molecular concepts and our proteomics data, we used the Oncomine Concepts Map bioinformatics tool developed and widely published by our group (39–43). Oncomine Concept Map (OCM) is the largest compendia of gene sets for association analysis. By computing the pairwise association among all the gene sets in the database, OCM allows for identification and visualization of "enrichment networks" of linked concepts. Such analysis enables us to link the class-specific protein profiles to over 14,000 molecular concepts, validating earlier observations and generating new hypothesis. Prior to performing the enrichment analysis for the proteomics data, a list of gene IDs was generated from the proteins that were determined to be differential (see "Statistical Analysis" above). This signature was used to seed the analysis. Once seeded, each pair of molecular concepts was tested for association using Fisher's exact test. Each concept was then analyzed independently, and the most significant concept was reported. Results were stored if a given test had an odds ratio >1.25 and a p value <0.01. Adjustment for multiple comparisons was made by computing Q values for all enrichment analyses (39). We are confident that the integrative analyses coupled to enrichment using OCM will generate a number of testable hypotheses on molecular events leading to development of cancer and its progression to advanced disease. For the analysis of class-specific proteomic profiles, all concepts that had a p value less than 0.001 were considered significant. A similar enrichment analysis of miR-128a gene expression profiles (see Fig. 4*e*) was carried out wherein the gene signature was determined by a Q value threshold of 5% on tests of differential expression. All concepts that had a p value less than 1×10^{-5} were considered significant.

Immunoblot Analysis

Proteins for immunoblotting were resolved by 4–12% NuPAGE gels (Invitrogen) and transferred to PVDF membranes (GE Healthcare). The membranes were blocked with 5% skimmed milk in TBS-T (20 mM Tris·Cl, pH 7.4, 150 mM NaCl, 0.1% Tween 20) overnight. Antibodies (indicated under "Antibodies") were added in TBS-T containing 2.5% skimmed milk, and the blots were washed with TBS-T. Immunoblot signals were developed using ECL reagent (GE Healthcare).

RNA Interference

Prostate epithelial cells (PrEC) or RWPE cells were treated with non-targeting small interfering RNA (D-001210-01, Dharmacon, Lafayette, CO) or small interfering RNA specific to miR-128 (D-003886-01, Dharmacon) according to published protocols (42, 43).

Quantitative RT-PCR

Q-PCR was performed using Power SYBR Green Mastermix on a 7300 Real Time PCR machine (both Applied Biosystems) as described previously (42). All primers were designed using Primer 3 and synthesized by Integrated DNA Technologies and are listed in supplemental Table 8. All PCR experiments were performed in triplicate.

MicroRNA Q-PCR

For microRNA quantitative PCR, total RNA including small RNA was isolated from prostate tissues and PrEC and DU145 cells that were transfected either with miR-128a (precursor human microRNA-128a), antagomiR-128a (44), or controls. Total RNA was used at 10 ng/μl. For RT, Mastermix was prepared using 0.15 μl of 100 mM dNTPs, 1.00 μl of MultiScribe reverse transcriptase (50 units/μl), 1.50 μl of 10$\times$ Reverse Transcription Buffer, 0.188 μl of RNase inhibitor

ASBMB MOLECULAR & CELLULAR PROTEOMICS MCP

(20 units/μl), and 4.192 μl of nuclease-free water. Each 15-μl RT reaction mixture contained 7 μl of Mastermix, 5 μl of RNA samples (10 ng/μl), and 3 μl of 5$\times$ specific RT primer. The thermal cycler was programmed as follows: 16 °C for 30 min, 42 °C for 30 min, and 85 °C for 5 min. Each PCR mixture contained 10 μl of TaqMan 2$\times$ Universal PCR Master Mix (No AmpErase UNG), 6.67 μl of nuclease-free water, 1 μl of 20$\times$ specific PCR primer, and 1.33 μl of RT products. Thr thermal cycler was programmed as follows: 95 °C for 10 min and 40 cycles of 95 °C for 15 s and 60 °C for 60 s. Using the comparative C_T method, we used endogenous control (RNU68) to normalize the expression levels of target microRNA by correcting differences in the amount of RNA loaded into Q-PCRs.

Cell Invasion Assay

Cell invasion was carried out using a modified basement membrane chamber assay as described previously (42). Briefly, equal numbers of the indicated cells were seeded onto the basement membrane matrix (extra cellular matrix, Chemicon) present in the insert of a 24-well culture plate with fetal bovine serum added to the lower chamber as a chemoattractant. After 48 h, non-invading cells and the endothelial cell matrix were removed by a cotton swab. Invaded cells were stained with crystal violet and photographed. The inserts were treated with 10% acetic acid, and absorbance was measured at 560 nm.

Cell Proliferation Assay

Cells were plated in 24-well plates at the desired cell concentration and transfected with precursor microRNA, antagomiR, or controls. After 48 h of transfection, cell counts were estimated by trypsinizing cells and analyses by Coulter counter (Beckman Coulter, Fullerton, CA) at the indicated time points in triplicate.

Gene Expression Analysis of Benign Prostate Epithelial Cells Attenuated for miR-128a Expression

Expression profiling of PrEC transfected ($n = 3$) with either control antagomiR (44) or antagomiR-128a was performed using the Illumina Whole Human Genome Bead Chip (Illumina, Hayward, Ca) according to the manufacturer's instructions. Total RNA isolated using TRIzol from the treated cells was purified using the Qiagen RNeasy Micro kit (Valencia, CA). Total RNA from control antagomiR-transfected PrEC was used as the reference. 1 μg of total RNA was converted to cRNA and hybridized according to the manufacturer's protocol (Illumina). Hybridizations were performed for 16 h at 65 °C, and arrays were scanned on an Agilent DNA microarray scanner. Images were analyzed, and data were extracted using Agilent Feature Extraction Software 9.1.3.1 with linear and lowess normalization performed for each array. A biological replicate was included for each of the two treatments. Correlation between the replicates was estimated using Pearson's correlation. A two-sided *t* test per probe followed by FDR calculation (Q value) was used to cull genes that were differential across the two treatment groups. Specifically, at a Q value threshold of 5%, 262 genes were found to be differential of which 181 were up-regulated upon miR-128a knockdown and the rest were down-regulated.

RESULTS

Quantitative Assessment of Prostate Cancer Proteome—An overview of the approach we took in quantifying proteomic alterations in prostate cancer is depicted in Fig. 1. In an effort to profile the proteome in the stages of prostate cancer progression, we used a combination of iTRAQ labeling and two-dimensional liquid chromatography coupled with mass spectrometry to interrogate the relative levels of proteins across 15 prostate-related biospecimens. The two-dimensional fractionation of the labeled peptides involved the use of an off-line SCX-based separation in the first dimension followed by an on-line reverse phase fractionation (Fig. 1). Each iTRAQ sample set was analyzed in three independent mass spectrometer runs (refer to "Experimental Procedures" for details). At a protein probability threshold of 0.955 (2% FDR), across the five iTRAQ sample sets, a total of 1221 and 1085 proteins were identified by two or more peptides using the two high capacity mass spectrometry runs, respectively, whereas the low capacity run yielded 967 proteins (supplemental Table 2 and Fig. S3). Among these, 777 proteins (56.6%) were shared across the three measurements (supplemental Fig. S3). There was 72.2% overlap in the proteins identified between the two high capacity runs and 66–69% overlap between any of the high capacity and the low capacity measurements (supplemental Fig. S3). Data from the three independent runs were first combined on a per sample basis using a weighted average, and the resulting compendium for each of the five iTRAQ sample sets was used for further analysis as described above. Overall, 1374 proteins were quantified across the biospecimens (refer to "Experimental Procedures" and supplemental Figs. S2 and S3 for analysis details) and identified by at least two unique peptides (in terms of amino acid sequence). Supplemental Fig. S4 shows a heat map representation of the 971 proteins that were measured in at least three of five iTRAQ experiments.

To delineate an organ-confined prostate cancer-specific proteomic signature, the data were first normalized by centering the trimmed mean of proteins in localized prostate cancer samples at 1 (upper and lower 10% of intensity values were excluded). Differentials were identified using a threshold set at 1.5 trimmed standard deviations from the trimmed mean. The final list of differentials was restricted to proteins that were concordantly differential in at least two or more samples in a given diagnostic class (see "Experimental Procedures" for details). A similar approach was used to define the metastatic prostate cancer-specific proteome relative to the localized prostate cancer except that in this case the sample trimmed mean and trimmed standard deviation were calculated by excluding 20% of the outliers in either direction. Furthermore, as we expect more spurious results due to differences in the site of metastasis, we required concordant results in at least 60% of the samples in which the protein was detected for further consideration. These class specific proteomic alterations are presented in a heat map format as described above (Fig. 2, *a* and *b*).

A total of 80 proteins was found to be elevated in PCA compared with Benign (Fig. 2*a*, *left panel*, and supplemental Table 3). Included among these were previously known alterations for prostate cancer, namely GOLM1 (45), transcription elongation factor B (SIII), polypeptide 1 (15 kDa; elongin C or

ASBMB MOLECULAR & CELLULAR PROTEOMICS MCP

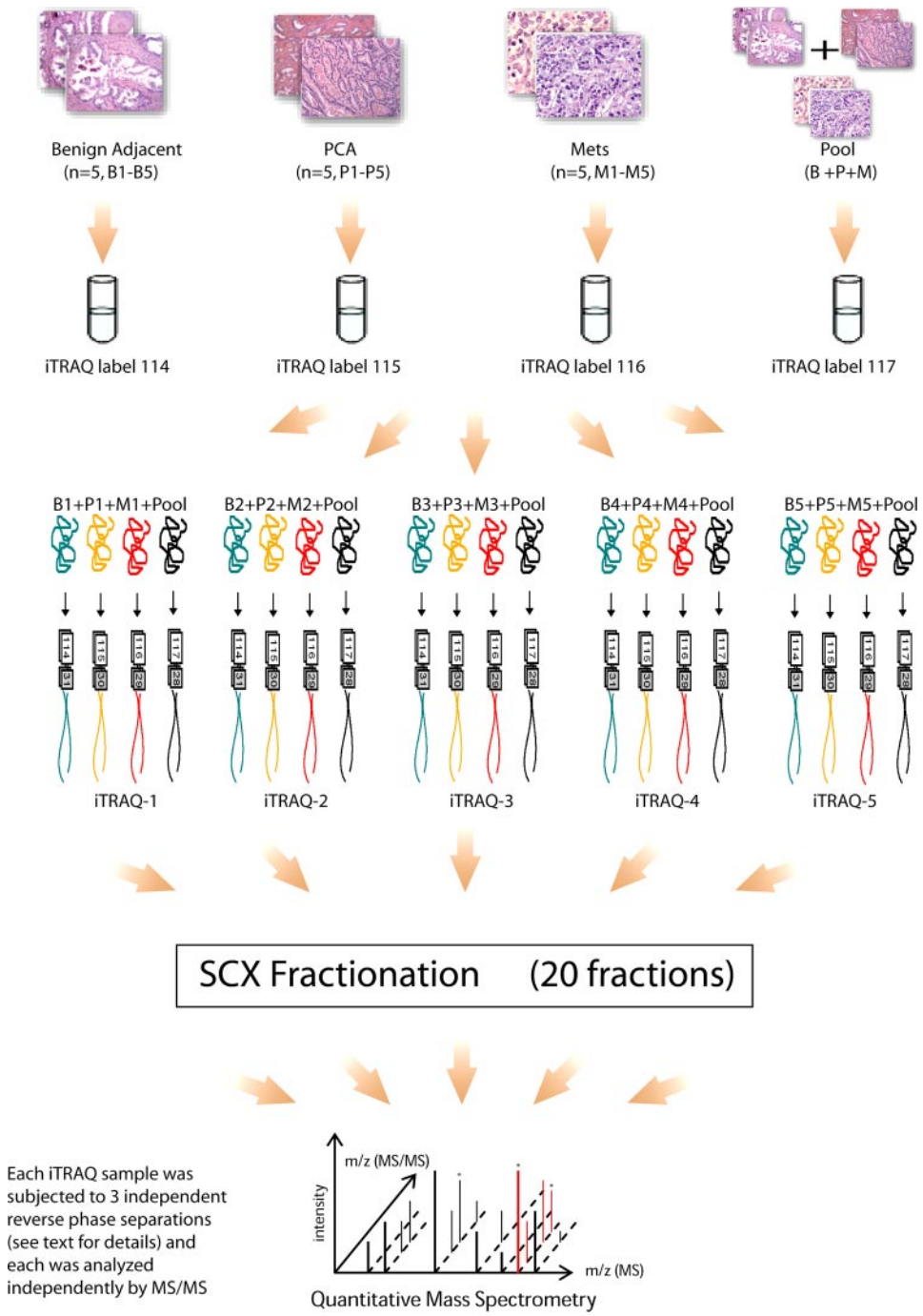

FIG. 1. **iTRAQ-based quantitative proteomic profiling of prostate cancer progression.** A flow chart of the steps involved in quantitative proteomic profiling of prostate-derived tissues is shown. This includes tissue procurement, histopathological examination, protein extraction, reduction, alkylation, trypsin digestion, iTRAQ labeling, peptide fractionation, and mass spectrometry-based detection and quantification. Each iTRAQ experiment consisted of tissues derived from Benign (*B*), localized cancer (PCA; *P*), and metastatic disease (Mets; *M*) labeled with isobaric tags 114, 115, and 116, respectively, whereas a pool containing equal amounts of tissue from all 15 prostate-derived samples used in the study was labeled using isobaric tag 117. The 4-plex mixture of peptides was separated using strong cation exchange chromatography, and the fractions were analyzed using MS/MS on a 6510 Agilent Q-TOF instrument after on-line reverse phase prefractionation on an HPLC-Chip. The spectral data were searched by X!Tandem using the human IPI database appended with reverse sequences. Statistical assessment of the search results used PeptideProphet and ProteinProphet. Quantitation was obtained using LIBRA.

ASBMB MOLECULAR & CELLULAR PROTEOMICS MCP

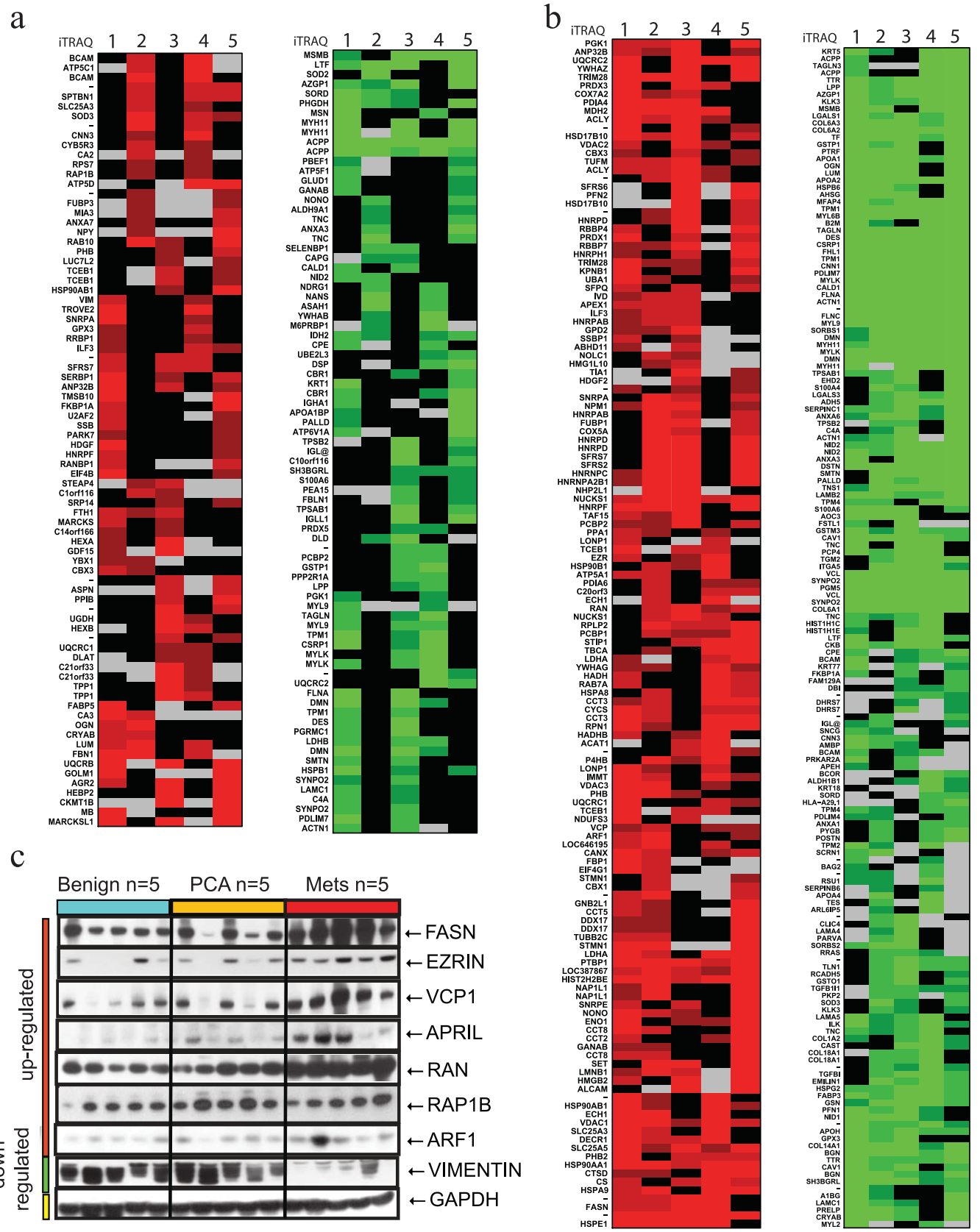
a
iTRAQ 1 2 3 4 5
BCAM
ATP5C1
BCAM
SPTBN1
SLC25A3
SOD3
CNN3
CYB5R3
CA2
RPS7
RAP1B
ATP5D
FUBP3
MIA3
ANXA7
NPY
RAB10
PHB
LUC7L2
TCEB1
TCEB1
HSP90AB1
VIM
TROVE2
SNRPA
GPX3
RRBP1
ILF3
SFRS7
SERBP1
ANP32B
TMSB10
FKBP1A
U2AF2
SSB
PARK7
HDGF
HNRPF
RANBP1
EIF4B
STEAP4
C1orf116
SRP14
FTH1
MARCKS
C14orf166
HEXA
GDF15
YBX1
CBX3
ASPN
PPIB
UGDH
HEXB
UQCRC1
DLAT
C21orf33
C21orf33
TPP1
TPP1
FABP5
CA3
OGN
CRYAB
LUM
FBN1
UQCRB
GOLM1
AGR2
HEBP2
CKMT1B
MB
MARCKSL1
iTRAQ 1 2 3 4 5
MSMB
LTF
SOD2
AZGP1
SORD
PHGDH
MSN
MYH11
MYH11
ACPP
ACPP
PBEF1
ATP5F1
GLUD1
GANAB
NONO
ALDH9A1
TNC
ANXA3
TNC
SELENBP1
CAPG
CALD1
NID2
NDRG1
NANS
ASAH1
YWHAB
M6PRBP1
IDH2
CPE
UBE2L3
DSP
CBR1
KRT1
CBR1
IGHA1
APOA1BP
PALLD
ATP6V1A
TPSB2
IGL@
C10orf116
SH3BGRL
S100A6
PEA15
FBLN1
TPSAB1
IGLL1
PRDX5
DLD
PCBP2
GSTP1
PPP2R1A
LPP
PGK1
MYL9
TAGLN
MYL9
TPM1
CSRP1
MYLK
MYLK
UQCRC2
FLNA
DMN
TPM1
DES
PGRMC1
LDHB
DMN
SMTN
HSPB1
SYNPO2
LAMC1
C4A
SYNPO2
PDLIM7
ACTN1
b
iTRAQ 1 2 3 4 5
PGK1
ANP32B
UQCRC2
YWHAZ
TRIM28
PRDX3
COX7A2
PDIA4
MDH2
ACLY
HSD17B10
VDAC2
CBX3
TUFM
ACLY
SFRS6
PFN2
HSD17B10
HNRPD
RBBP4
PRDX1
RBBP7
HNRPH1
TRIM28
KPNB1
UBA1
SFPQ
APEX1
ILF3
HNRPAB
GPD2
SSBP1
ABHD11
NOLC1
HMG1L10
TIA1
HDGF2
SNRPA
NPM1
HNRPAB
FUBP1
COX5A
HNRPD
HNRPD
SFRS7
SFRS2
HNRNPC
HNRNPA2B1
NHP2L1
NUCKS1
HNRPF
TAF15
PCBP2
PPA1
LONP1
TCEB1
EZR
HSP90B1
ATP5A1
PDIA6
C20orf3
ECH1
RAN
NUCKS1
RPLP2
PCBP1
STIP1
TBCA
LDHA
YWHAG
HADH
RAB7A
HSPA8
CCT3
CYCS
CCT3
RPN1
HADHB
ACAT1
P4HB
LONP1
IMMT
VDAC3
PHB
UQCRC1
TCEB1
NDUFS3
VCP
ARF1
LOC646195
CANX
FBP1
EIF4G1
STMN1
CBX1
GNB2L1
CCT5
DDX17
DDX17
TUBB2C
STMN1
LDHA
PTBP1
LOC387867
HIST2H2BE
NAP1L1
NAP1L1
SNRPE
NONO
ENO1
CCT8
CCT2
GANAB
CCT8
SET
LMNB1
HMGB2
ALCAM
HSP90AB1
ECH1
VDAC1
SLC25A3
DECR1
SLC25A5
PHB2
HSP90AA1
CTSD
CS
HSPA9
FASN
HSPE1
iTRAQ 1 2 3 4 5
KRT5
ACPP
TAGLN3
ACPP
TTR
LPP
AZGP1
KLK3
MSMB
LGALS1
COL6A3
COL6A2
TF
GSTP1
PTRF
APOA1
OGN
LUM
APOA2
HSPB6
AHSG
MFAP4
TPM1
MYL6B
B2M
TAGLN
DES
CSRP1
FHL1
TPM1
CNN1
PDLIM7
MYLK
CALD1
FLNA
ACTN1
FLNC
MYL9
SORBS1
DMN
MYH11
MYLK
DMN
MYH11
TPSAB1
EHD2
S100A4
LGALS3
ADH5
SERPINC1
ANXA6
TPSB2
C4A
ACTN1
NID2
NID2
ANXA3
DSTN
SMTN
PALLD
TNS1
LAMB2
TPM4
S100A6
AOC3
FSTL1
GSTM3
CAV1
TNC
PCP4
TGM2
ITGA5
VCL
SYNPO2
PGM5
VCL
SYNPO2
COL6A1
TNC
HIST1H1C
HIST1H1E
LTF
CKB
CPE
BCAM
KRT77
FKBP1A
FAM129A
DBI
DHRS7
DHRS7
IGL@
SNCG
CNN3
AMBP
BCAM
PRKAR2A
APEH
BCOR
ALDH1B1
KRT18
SORD
HLA-A29.1
TPM4
PDLIM4
ANXA1
PYGB
POSTN
TPM2
SCRN1
BAG2
RSU1
SERPINB6
APOA4
TES
ARL6IP5
CLIC4
LAMA4
PARVA
SORBS2
RRAS
TLN1
RCADH5
GSTO1
TGFB1I1
PKP2
SOD3
KLK3
LAMA5
ILK
TNC
COL1A2
CAST
COL18A1
COL18A1
TGFBI
EMILIN1
HSPG2
FABP3
GSN
PFN1
NID1
APOH
GPX3
COL14A1
BGN
TTR
CAV1
BGN
SH3BGRL
A1BG
LAMC1
PRELP
CRYAB
MYL2
c
Benign n=5
PCA n=5
Mets n=5
up-regulated
down-regulated
FASN
EZRIN
VCP1
APRIL
RAN
RAP1B
ARF1
VIMENTIN
GAPDH

ASBMB MOLECULAR & CELLULAR PROTEOMICS MCP

TCEB1) (46), neuropeptide Y (47), Parkinson disease (autosomal recessive, early onset) 7 (PARK7 or DJ-1) (48), anterior gradient homolog-2 (AGR2) (49), growth differentiation factor 15 (GDF15, MIC-1, or NAG-1) (50), ferritin heavy chain (FTH1) (51), tumor necrosis factor, α-induced protein 9 (STAMP2 or STEAP4) (52), fatty acid-binding protein (FABP5) (53), and VIM (54). A similar analysis for down-regulated proteins revealed 81 proteins whose expression was decreased in PCA compared with Benign (Fig. 2*a*, *right panel*, and supplemental Table 4). Prominent among these were lactotransferrin (55), α_2-glycoprotein (AZGP1) (56), microseminoprotein β (prostatic secretory protein of 94 amino acids, PSP94, or MSMB) (57), isoforms of glutathione transferase (GSTP1 and GSTM3) (58–60), lactate dehydrogenase B (61), and N-myc downstream regulated gene (NDRG1) (62), all of which have been reported earlier to be down-regulated in organ-confined disease.

Furthermore, our analysis revealed, for the first time, additional proteins that were dysregulated in organ-confined disease (PCA) compared with Benign controls. These included elevated levels of the leucine-rich proteins Asporin and acidic (leucine-rich) nuclear phosphoprotein 32 family, member B (ANP32B or APRIL); GTP-binding proteins like RAB10, Ran-binding protein 1 (RANBP1), and RAP1B; and DNA-binding proteins like Y-box-binding protein 1 (YBX1) and chromobox homolog 3 (CBX3; Fig. 2*a*, *left panel*). Similarly, the quantitative approach revealed tumor-associated down-regulation of multiple cytoskeletal and extracellular matrix-associated proteins like Desmuslin, Actinin α1 (ACTN1), Tropomyosin 1 (TPM1), Filamin A, and Nidogen A (NID2) and LIM domain-containing proteins like LPP and PDLIM7 (Fig. 2*a*, *right panel*).

Likewise, 141 and 165 proteins were found to be elevated and down-regulated, respectively, in metastatic disease (Mets) compared with organ-confined cancer (PCA; Fig. 2*b* and supplemental Tables 5 and 6). Included in these were proteins that have been previously reported to be perturbed in advanced disease as well those found to be dysregulated by our study (Fig. 2*b*). Included in the former were enzymes like phosphoglycerate kinase 1 (PGK1) (63), hydroxysteroid (17-β) dehydrogenase (HSD17B) (64), enolase 1α (ENO1/MBP1) (65), acetyl-coenzyme A acetyltransferase 1 (ACAT1) (66), and fructose-1,6-bisphosphatase 1 (FBP1) (67); oncogenes like stathmin 1/oncoprotein 18 (STMN1) (68); and signaling molecules like 14−3−3 protein (YWHAZ) (65) and a member of the RAS oncogene family (RAN) (69) among others (Fig. 2*b*, *left panel*). Additionally, our profiling study, for the first time, revealed elevated levels of proteins belonging to solute carrier family like SLC25A3 and SLC25A5; splicing factors, namely arginine/serine-rich 2 (SFRS2) and splicing factor, arginine/serine-rich 7 (SFRS7); and chaperonins containing TCP1 complex like CCT2, CCT3, CCT5, and CCT8 in metastatic disease compared with organ-confined tumors (Fig. 2*b*, *left panel*). Included among the proteins that were down-regulated and reported previously were S100A6 (70), superoxide dismutase 3 (SOD3) (71), transforming growth factor, β1 (TGFB-1) (72), destrin (73), gelsolin (74), and the lectin galactoside-binding, soluble, 3 (LGALS3) (75) (Fig. 2*b*, *right panel*, and supplemental Table 6).

We further validated some of these proteomic alterations using immunoblot analysis carried out on independent prostate-related specimens (five each of Benign, PCA and Mets; Fig. 2*c*). As shown in Fig. 2*c*, elevated levels of fatty-acid synthase, Ezrin, VCP1, APRIL (ANP32B), RAN, RAP1B, and ARF1 were validated in localized tumors and metastatic disease. Also, VIM, which was largely down-regulated in metastatic samples, was confirmed using independent clinical specimens (Fig. 2*c*). Having validated our mass spectrometry results, we were interested in delineating the biological nuance associated with these proteomic alterations. Toward this, we carried out an enrichment analysis of the localized prostate cancer-specific proteomic signature.

Analysis of Prostate Cancer-associated Biological Processes and Pathways by OCM—To determine the ability of our PCA-specific signature to identify pathways that are deregulated during prostate cancer development and progression, we performed an OCM analysis on the group of proteins that were identified to be up-regulated in organ-confined disease (PCA) compared with Benign (see "Experimental Procedures" and supplemental Table 3 for a list of proteins used). Our laboratory's recent work in the enrichment analysis of biologically related gene sets allows for the discovery of patterns of shared behavior over a vast database of high throughput experimental data and biological annotation (40). The 80 proteins that were elevated in PCA mapped to 72 gene symbols that were analyzed by OCM. The enrichment analysis was performed against a null set containing 1143 gene symbols associated with the 1374 proteins identified across the 15 iTRAQ experiments, allowing the selection of specific concepts enriched by the differential predictor. The OCM analysis of the "PCA-specific protein" signature (center green node) showed enrichment for multiple Oncomine gene signatures (blue nodes) describing an increase in prostate cancer (p =

FIG. 2. **Class-specific proteomic profiles of prostate cancer progression.** *a*, heat map showing differential proteins in PCA relative to benign samples (see "Experimental Procedures" for details). Gene symbols are listed when known. *Rows* represent the proteins, and *columns* represent the five iTRAQ experiments. Up-regulated and down-regulated proteins are indicated in shades of *red* and *green*, respectively, where the intensity of the color is determined by the distance (in standard deviations) from the mean of the trimmed distribution. *Black* indicates unchanged protein expression, and *gray* indicates no measurement. *b*, same as in *a* but for differential proteins in metastatic disease compared with localized tumors. *c*, immunoblot validation of candidate proteins in an independent set of prostate-derived samples (n = 5 from each class). *FASN*, fatty-acid synthase; *GAPDH*, glyceraldehyde-3-phosphate dehydrogenase.

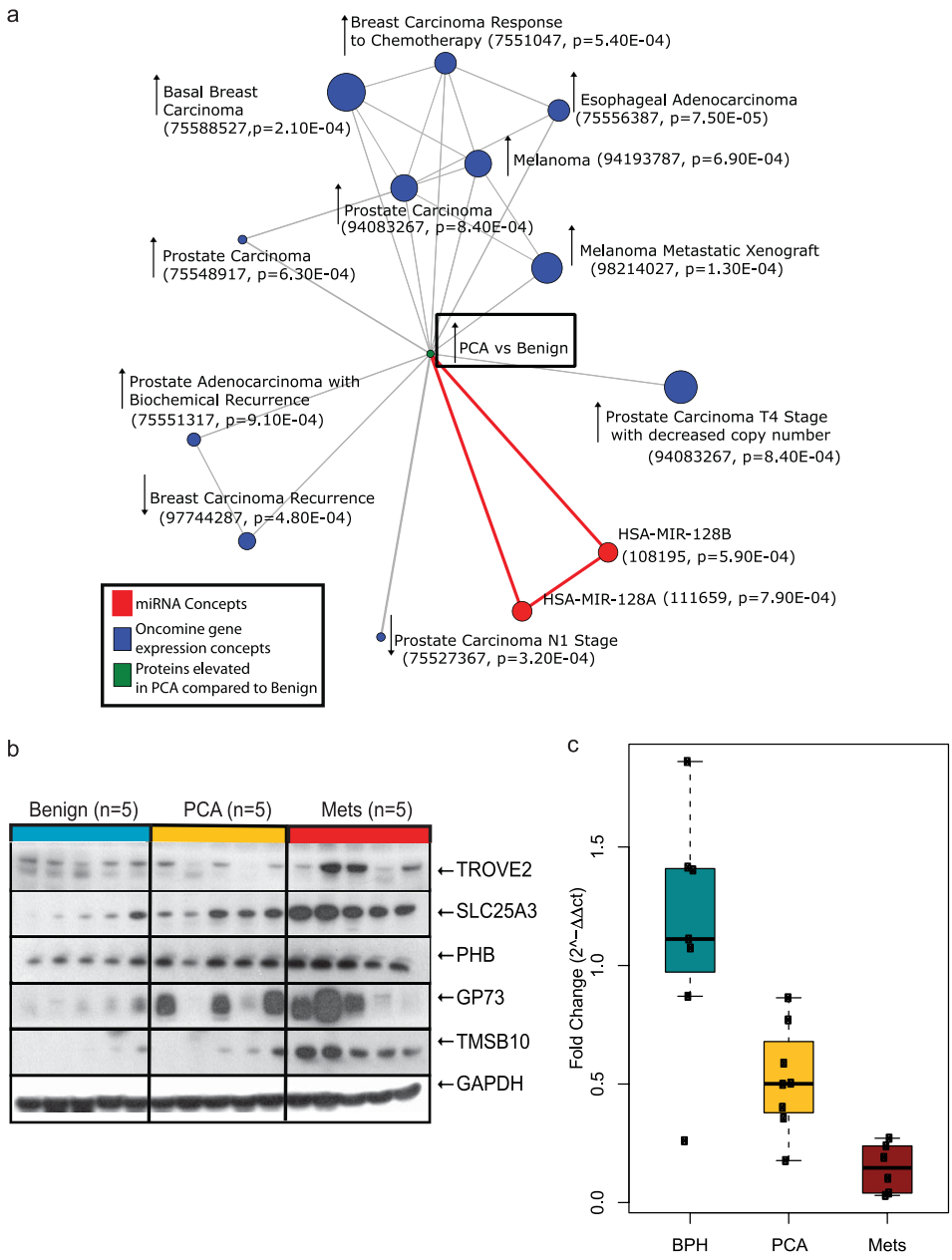

FIG. 3. **Integrative analysis of localized prostate cancer-specific proteomic profiles and delineation of a potential role for miR-128 in prostate cancer.** *a*, network view of the molecular concept analysis for the proteomic profiles of our overexpressed in the "PCA *versus* Benign" signature (*center green node*). Each *node* represents a molecular concept or a set of biologically related genes. The *node size* is proportional to the number of genes in the concept. Each *edge* represents a statistically significant enrichment ($p < 1 \times 10^{-3}$). Enrichments with interconnected "HSA-MIR-128," indicating involvement of miR-128 regulation in PCA *versus* Benign, are indicated by *red nodes*. *b*, immunoblot validation of candidate proteins in the overexpressed in the PCA *versus* Benign signature that enriched for miR-128 concept in *a*. *c*, box plot showing -fold change of miR-128 expression in prostate-derived tissues (seven BPH, eight PCA, and six Mets), relative to the average BPH expression, assessed by Q-PCR. For each box plot, the median value is represented by the *central*, *horizontal line*; the upper (75%) and lower (25%) quartiles are represented by the *upper* and *lower borders* of the *box*. The *upper* and *lower vertical lines* extending from the *box* extend to the farthest measures within 1.5 times the interquartile range from the upper and lower quartiles. *miRNA*, microRNA; *GAPDH*, glyceraldehyde-3-phosphate dehydrogenase.

6.3×10^{-4} and $p = 9.8 \times 10^{-4}$), esophageal cancer ($p = 7.5 \times 10^{-5}$), melanoma ($p = 6.9 \times 10^{-4}$), and basal-like breast cancers ($p = 2.1 \times 10^{-4}$). Additionally, picTAR-derived microRNA concepts (red edges and nodes) implicating miR-128a (HSA-MIR-128A; $p = 7.9 \times 10^{-4}$) and miR-128b (HSA-MIR-128B; $p = 5.9 \times 10^{-4}$) in prostate cancer development (see Fig. 3*a* and supplemental Table 7 for a list of all concepts within the *p* value threshold of 1×10^{-3}). This miR-128 concept

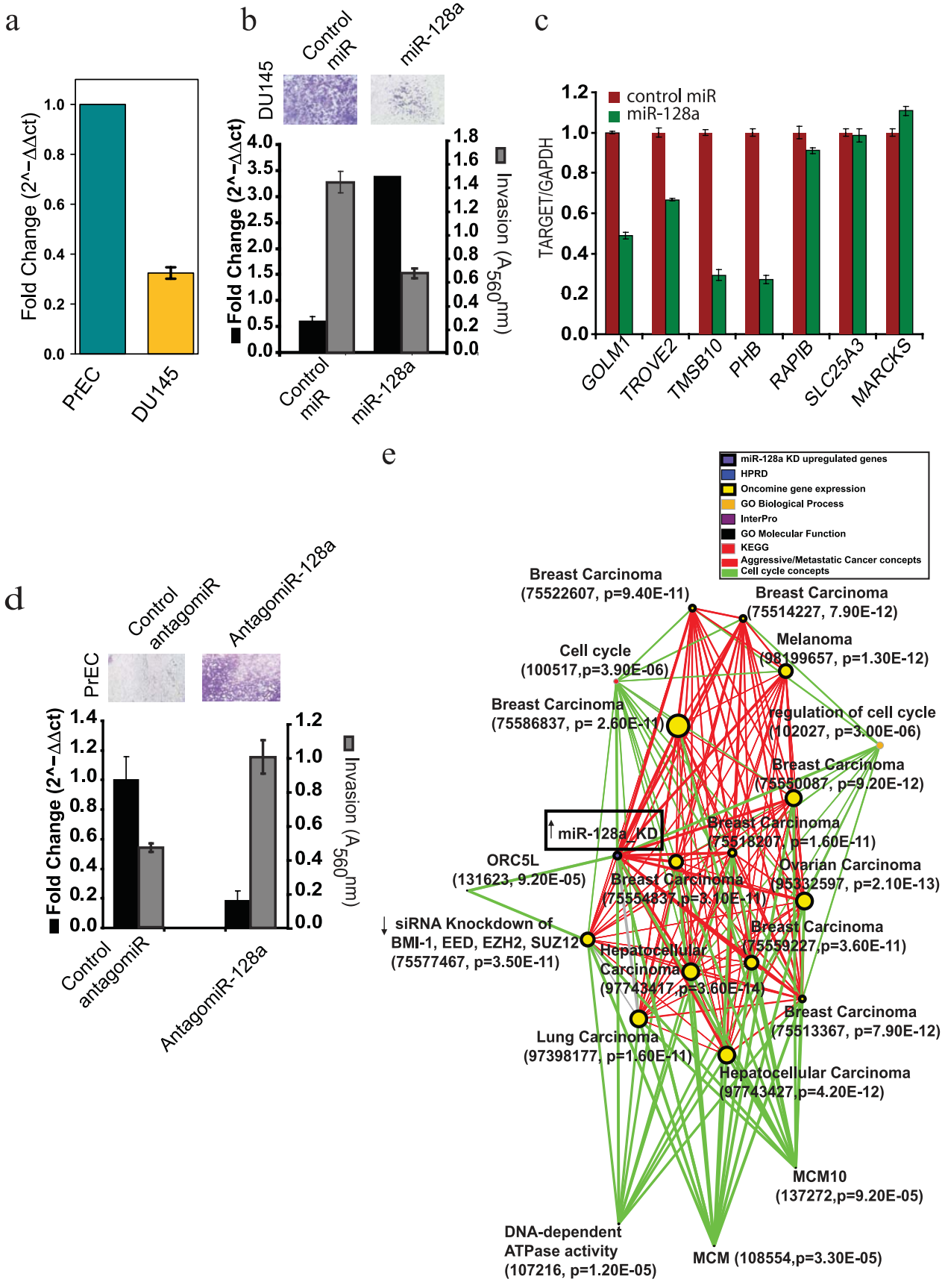
a
Fold Change (2^−ΔΔct)
PrEC
DU145
b
Control miR
miR-128a
DU145
Fold Change (2^−ΔΔct)
Invasion (A560nm)
Control miR
miR-128a
c
control miR
miR-128a
TARGET/GAPDH
GOLM1
TROVE2
TMSB10
PHB
RAPIB
SLC25A3
MARCKS
d
Control antagomiR
AntagomiR-128a
PrEC
Fold Change (2^−ΔΔct)
Invasion (A560nm)
Control antagomiR
AntagomiR-128a
e
miR-128a KD upregulated genes
HPRD
Oncomine gene expression
GO Biological Process
InterPro
GO Molecular Function
KEGG
Aggressive/Metastatic Cancer concepts
Cell cycle concepts
Breast Carcinoma (75522607, p=9.40E-11)
Breast Carcinoma (75514227, 7.90E-12)
Cell cycle (100517,p=3.90E-06)
Melanoma (98199657, p=1.30E-12)
Breast Carcinoma (75586837, p= 2.60E-11)
regulation of cell cycle (102027, p=3.00E-06)
Breast Carcinoma (75590087, p=9.20E-12)
↑miR-128a_KD
Breast Carcinoma (75518207, p=1.60E-11)
ORC5L (131623, 9.20E-05)
Ovarian Carcinoma (95332597, p=2.10E-13)
Breast Carcinoma (75554837,p=3.10E-11)
↓siRNA Knockdown of BMI-1, EED, EZH2, SUZ12 (75577467, p=3.50E-11)
Breast Carcinoma (75559227,p=3.60E-11)
Hepatocellular Carcinoma (97743417,p=3.60E-11)
Breast Carcinoma (75513367, p=7.90E-12)
Lung Carcinoma (97398177, p=1.60E-11)
Hepatocellular Carcinoma (97743427,p=4.20E-12)
MCM10 (137272,p=9.20E-05)
DNA-dependent ATPase activity (107216, p=1.20E-05)
MCM (108554,p=3.30E-05)

was intriguing in the context of a recent study that predicted a decrease in the expression of this microRNA in breast cancer (76). However, the functional consequence of this down-regulation has not been described thus far. This motivated us to extend our investigation to understand the consequence of miR-128 deregulation in the context of prostate cancer.

Assessment of miR-128 Expression in Prostate-derived Tissues and Cell Lines—miR-128 concepts were enriched in our OCM analysis by eight high confidence proteins (all identified by at least two peptides), namely GOLM1, TROVE2, PHB, solute carrier family 25 (SLC25A3), myristoylated alanine-rich protein kinase C substrate, heteronuclear ribonucleoprotein (HNRPF), TMSB10, and a member of RAS oncogene family (RAP1B), all of which were elevated in localized prostate cancer and further were predicted to be targets of the microRNA by picTAR. Toward characterizing the role of miR-128, we first validated the expression of GOLM1, PHB, TROVE2, TMSB10, and SLC25A3 in independent clinical specimens ($n = 5$ each of Benign, PCA, and Mets) using immunoblot analysis (Fig. 3*b*). Next, we confirmed deregulation of miR-128 expression in independent clinical specimens using real time PCR analysis (refer to supplemental Table 8 for the sequences of primers used). Analysis of 21 independent clinical specimens (seven benign prostatic hyperplasia/BPH, eight PCA, and six Mets) revealed significant reduction in expression of miR-128 in a progressive fashion from BPH to PCA to metastatic disease (Fig. 3*c*; $p = 0.0163$ PCA *versus* BPH, $p = 0.0017$ PCA *versus* Mets).

Specifically, transcript levels for miR-128 were significantly decreased in PCA compared with BPH samples (*t* test with Satterthwaite correction for unequal variances, $p = 0.016$). Additionally, miR-128 transcript levels displayed an even greater down-regulation in the metastatic samples compared with organ-confined disease (Fig. 3*c*; $p = 0.0017$).

To determine whether miR-128 down-regulation in prostate cancer has biological relevance, we used prostate cancer cell line DU145 and its benign epithelial counterpart, primary benign PrEC. Using these cell lines, we assessed their transcript levels for miR-128 using Q-PCR. As shown in Fig. 4*a*, the prostate cancer cell line DU145 displayed lower levels of miR-128 (one-sample *t* test, $p = 0.0002$, $n = 3$) compared with their benign epithelial counterparts. This was in line with our earlier observation with prostate tissues wherein a decrease in expression of the microRNA correlated with aggressivity of the disease.

This finding motivated us to interrogate the functional role of miR-128 in prostate cancer development/progression. We performed transient overexpression or knockdown of the microRNA in prostate cancer and benign prostate epithelial cells, respectively, and looked for changes in cell proliferation/invasion. Cell proliferation and cellular invasion were correspondingly measured using cell counting and a modified Boyden chamber matrigel invasion assay (77). Interestingly, transient overexpression of miR-128a in the invasive prostate cancer cell line DU145 resulted in >50% attenuation of invasion (Fig. 4*b*), confirming our earlier prediction of a role for miR-128 in regulating prostate cancer aggressivity. No change in cell numbers was detected between treatments (see supplemental Fig. S5). Furthermore, these attenuated cells showed decreased expression for four of the seven predicted target genes (*GOLM1*, *PHB*, *TROVE2*, and *TMSB10*) that nominated the miR-128 in our enrichment analysis (Fig. 4*c*). Importantly, this observation suggests the associated proteins as genuine targets of miR-128, although additional study is necessary for confirmation. To further confirm the role of miR-128 in regulating cancer aggressivity, we knocked down its expression using specific antagomiR in benign PrEC. As shown in Fig. 4*d*, transient transfection of antagomiR resulted in an ~80% reduction in miR-128 transcript levels compared with non-target control (Fig. 4*d*, *black bars*). Furthermore, this attenuation of miR-128 was accompanied by induction of the invasive phenotype in these benign epithelial cells (Fig. 4*d*, *gray bars*). Invasion was not induced by control or mock antagomiR

FIG. 4. **miR-128 is associated with prostate cancer invasion and aggressivity.** *a*, assessment of miR-128 expression in a benign prostate epithelial cell line (PrEC) and a prostate cancer cell line (DU145) by Q-PCR ($n = 3$; fold change relative to PrEC expression per experiment). *b*, assessment of invasion in prostate cancer cells (DU145) upon overexpression of miR-128a. Transcript levels (*black bars*) and invasion (*gray bars*) were assessed by Q-PCR and a Boyden chamber assay, respectively. *Error bars* are derived from two biological replicate measures. Overexpression of miR-128a in invasive DU145 cells resulted in a >2-fold decrease in invasiveness compared with control miR-transfected cells (see *inset* for photomicrograph of invasion). *c*, assessment of relative levels of transcripts for seven of the eight genes that enriched for the miR-128 concept in Fig. 3*a* upon overexpression of the microRNA in invasive DU145 cells ($n = 3$). Overexpression of miR-128a in DU145 cells resulted in a concomitant down-regulation of *GOLM1*, *TROVE2*, *TMSB10*, and *PHB*, further suggesting them as downstream targets of the microRNA. Levels of *RAP1B*, *SLC25A3*, and myristoylated alanine-rich protein kinase C substrate (*MARCKS*) were unchanged. *d*, same as in *b* but for knockdown of miR-128a in primary PrEC compared with antagomiR control. Attenuation of miR-128a levels (*black bars*) resulted in a concomitant induction of an invasive phenotype (*gray bars* and *inset*) in primary prostate epithelial cells. *Error bars* are derived from three biological replicates. *e*, network view of the molecular concept analysis for the gene expression profiles of our up-regulated upon "mir-128a knockdown" signature (*miR-128a_KD*). Each *node* represents a molecular concept or a set of biologically related genes. The *node size* is proportional to the number of genes in the concept. Each *edge* represents a statistically significant enrichment ($p < 1 \times 10^{-5}$). Multiple enrichments for aggressive/metastatic cancers (*red bridges*) confirm a role for miR-128a in regulating invasiveness/aggressivity of tumors. Also, multiple enrichments of cell cycle-related concepts (*green bridges*) confirm earlier findings for a role of miR-128a in regulation of this biological process (78). *GAPDH*, glyceraldehyde-3-phosphate dehydrogenase; *HRPD*, Human Protein Reference Database; *KEGG*, Kyoto Encyclopedia of Genes and Genomes; *GO*, Gene Ontology; MCM, Mini-chromosome Maintenance.

ASBMB MOLECULAR & CELLULAR PROTEOMICS MCP

ASBMB MOLECULAR & CELLULAR PROTEOMICS MCP

treatments (see supplemental Fig. S6). Similar induction of the invasive phenotype accompanying an attenuation of miR-128 levels was also observed using an independent benign transformed epithelial cell line (RWPE; data not shown). These validated a role for miR-128 in regulating tumor invasion.

To get additional insights, we carried out gene expression analysis of benign PrEC upon overexpression of miR-128a. Genes that were down-regulated upon the overexpression of the microRNA were used for enrichment analysis using Oncomine Concepts Map (39, 40) (refer to Fig. 4*e* and supplemental Table 9 for a list of all concepts within the p value threshold of 1×10^{-5}). Included in the list of concepts enriched by the "miR-128a targets" (Fig. 4*e*, *miR-128a_KD*) were those that described regulation of cell cycle (Fig. 4*e*, *green bridges*). Notably, this served as a reference for our analysis as earlier reports have confirmed a role for miR-128 in cell cycle regulation through its control of *E2F3* expression (78). Of more interest to us, however, was the enrichment of multiple concepts, all of which described invasive tumors or those with poor outcome (Fig. 4*e*, *red bridges*). These included gene expression-derived concepts for aggressive tumors of breast, lung, liver, and ovary (Fig. 4*e*, *red bridges*). This observation further strengthened our *in vitro* findings implicating miR-128 in cancer aggressivity, especially the process of tumor invasion.

DISCUSSION

By coupling multidimensional protein fractionation and quantitative mass spectrometry with bioinformatics-based enrichment analysis, we demonstrate the involvement of miR-128 in the stages of prostate cancer progression. The proteomic signatures quantified in both organ-confined and metastatic samples contained proteins that have been previously implicated in this disease. Significant among these were multiple proteins belonging to the secretory or endocytic pathways. This included the Golgi-associated antigen GOLM1, which has been recently reported from our laboratory to be elevated both at the transcript and protein levels in localized tumors (45). Similarly, STEAP4, known to be androgen-regulated and involved in endocytic trafficking (52), was elevated in localized tumors. An important finding from our profiling data was the elevation in levels of multiple proteins that contain leucine-rich protein-interacting motifs (Asporin and APRIL or ANP32B). The protein PP32R1, a member of the ANP32 family, has been shown to be oncogenic with very high levels of expression in prostate adenocarcinoma cell lines (79). Additional findings from our data included elevated levels of DNA-binding and GTP-binding proteins, confirming increased transcriptional activity and signaling, respectively, during early cancer development. The metastatic signature, on the other hand, showed elevated levels of multiple arginine-serine-rich pre-mRNA splicing factors. This is relevant in the context of existing knowledge that implicates these in cancer development (80). Also our "Up in Metastatic" signature revealed elevated levels of solute carrier proteins, namely SLC25A5 and SLC25A3. The former has been implicated earlier to be elevated in lymph node metastasis associated with hepatocellular carcinoma (81), whereas SLC25A3 serves as the mitochondrial transporter for phosphate (82). Interestingly, independent metabolomics data for prostate cancer progression generated by our laboratory revealed significantly elevated levels of inorganic phosphate in tumors, corroborating with the finding of elevated levels of phosphate carrier in metastatic prostate cancer (83).

Importantly, extending beyond revealing single molecule alterations, we interrogated the biological significance of these alterations in the context of prostate cancer development/progression using OCM. An enrichment of miR-128 concepts by the tumor-specific signature was revealed. This was exciting because studies from our laboratory and others have implicated microRNAs in regulating tumor progression (84) and invasiveness (85). Remarkably, to our knowledge, this is one of the first studies wherein mass spectrometry-based protein profiling has been combined with bioinformatics-driven enrichment to nominate a microRNA in tumors. Importantly, our study, for the first time, implicates miR-128 in prostate cancer. Our results from *in vitro* transient overexpression and knockdown systems indicate a role for miR-128 in prostate cancer invasion. This is further strengthened by the OCM analysis of miR-128-regulated genes that showed enrichment for multiple concepts describing aggressive tumors or those having poor outcome. Taken together, we combined quantitative protein mass spectrometry, bioinformatics, and a cell-based functional assay to delineate a role for miR-128 in prostate cancer progression.

Acknowledgment—We thank Dr. Kenneth Pienta for access to metastatic prostate cancer samples from the University of Michigan Prostate Specialized Project of Research Excellence rapid autopsy program.

* This work was supported, in whole or in part, by National Institutes of Health Grants R01CA13345 (to A. S. and A. M. C.), R03CA139489 (to A. S.), and R01CA126239 (to A. I. N.); Specialized Project of Research Excellence Grant P50 CA69568 (to A. M. C.); and Early Detection Research Network Grant U01 CA113913 (to A. M. C.) from the NCI. This work was also supported by Department of Defense Grant W81XWH-06-1-0224 (to A. M. C.) and Michigan Technology Tri-Corridor Grant MTTC-687 (to A. S. and G. S. O.).

S The on-line version of this article (available at http://www.mcponline.org) contains supplemental Figs. S1–S6 and Tables 1–9.

c Both authors contributed equally to this work.

f Present address: Agilent Technologies, Wilmington, DE 19808.

l Supported by a clinical translational science award from the Burroughs Welcome Foundation and Doris Duke Charitable Foundation.

m Supported by a Georgia cancer research distinguished scientist award. To whom correspondence should be addressed: Medical College of Georgia Cancer Center, CN3130, 1420 Laney Walker Blvd., Augusta, GA 30912. Tel.: 706-721-0097; Fax: 706-721-1670; E-mail: asreekumar@mcg.edu.

ASBMB MOLECULAR & CELLULAR PROTEOMICS MCP

REFERENCES

1. American Cancer Society (2008) *How Many Men Get Prostate Cancer?*, American Cancer Society, Atlanta, GA
2. Catalona, W. J. (1994) Management of cancer of the prostate. *N. Engl. J. Med.* **331,** 996–1004
3. Jacobsen, S. J., Katusic, S. K., Bergstralh, E. J., Oesterling, J. E., Ohrt, D., Klee, G. G., Chute, C. G., and Lieber, M. M. (1995) Incidence of prostate cancer diagnosis in the eras before and after serum prostate-specific antigen testing. *JAMA* **274,** 1445–1449
4. Epstein, J. I., and Potter, S. R. (2001) The pathological interpretation and significance of prostate needle biopsy findings: implications and current controversies. *J. Urol.* **166,** 402–410
5. Andriole, G. L., Crawford, E. D., Grubb, R. L., 3rd, Buys, S. S., Chia, D., Church, T. R., Fouad, M. N., Gelmann, E. P., Kvale, P. A., Reding, D. J., Weissfeld, J. L., Yokochi, L. A., O'Brien, B., Clapp, J. D., Rathmell, J. M., Riley, T. L., Hayes, R. B., Kramer, B. S., Izmirlian, G., Miller, A. B., Pinsky, P. F., Prorok, P. C., Gohagan, J. K., and Berg, C. D. (2009) Mortality results from a randomized prostate-cancer screening trial. *N. Engl. J. Med.* **360,** 1310–1319
6. Schröder, F. H., Hugosson, J., Roobol, M. J., Tammela, T. L., Ciatto, S., Nelen, V., Kwiatkowski, M., Lujan, M., Lilja, H., Zappa, M., Denis, L. J., Recker, F., Berenguer, A., Määttänen, L., Bangma, C. H., Aus, G., Villers, A., Rebillard, X., van der Kwast, T., Blijenberg, B. G., Moss, S. M., de Koning, H. J., and Auvinen, A. (2009) Screening and prostate-cancer mortality in a randomized European study. *N. Engl. J. Med.* **360,** 1320–13208
7. Albertsen, P. C., Hanley, J. A., Gleason, D. F., and Barry, M. J. (1998) Competing risk analysis of men aged 55 to 74 years at diagnosis managed conservatively for clinically localized prostate cancer. *JAMA* **280,** 975–980
8. Brown, C., Sauvageot, J., Kahane, H., and Epstein, J. I. (1996) Cell proliferation and apoptosis in prostate cancer—correlation with pathologic stage? *Mod. Pathol.* **9,** 205–209
9. Abate-Shen, C., and Shen, M. M. (2000) Molecular genetics of prostate cancer. *Genes Dev.* **14,** 2410–2434
10. Kumar-Sinha, C., and Chinnaiyan, A. M. (2003) Molecular markers to identify patients at risk for recurrence after primary treatment for prostate cancer. *Urology* **62,** Suppl. 1, 19–35
11. Hood, L., Heath, J. R., Phelps, M. E., and Lin, B. (2004) Systems biology and new technologies enable predictive and preventative medicine. *Science* **306,** 640–643
12. Grubb, R. L., Calvert, V. S., Wulkuhle, J. D., Paweletz, C. P., Linehan, W. M., Phillips, J. L., Chuaqui, R., Valasco, A., Gillespie, J., Emmert-Buck, M., Liotta, L. A., and Petricoin, E. F. (2003) Signal pathway profiling of prostate cancer using reverse phase protein arrays. *Proteomics* **3,** 2142–2146
13. Petricoin, E. F., 3rd, Ornstein, D. K., Paweletz, C. P., Ardekani, A., Hackett, P. S., Hitt, B. A., Velassco, A., Trucco, C., Wiegand, L., Wood, K., Simone, C. B., Levine, P. J., Linehan, W. M., Emmert-Buck, M. R., Steinberg, S. M., Kohn, E. C., and Liotta, L. A. (2002) Serum proteomic patterns for detection of prostate cancer. *J. Natl. Cancer Inst.* **94,** 1576–1578
14. Paweletz, C. P., Charboneau, L., Bichsel, V. E., Simone, N. L., Chen, T., Gillespie, J. W., Emmert-Buck, M. R., Roth, M. J., Petricoin, E. F., 3rd, and Liotta, L. A. (2001) Reverse phase protein microarrays which capture disease progression show activation of pro-survival pathways at the cancer invasion front. *Oncogene* **20,** 1981–1989
15. Dhanasekaran, S. M., Barrette, T. R., Ghosh, D., Shah, R., Varambally, S., Kurachi, K., Pienta, K. J., Rubin, M. A., and Chinnaiyan, A. M. (2001) Delineation of prognostic biomarkers in prostate cancer. *Nature* **412,** 822–826
16. Lapointe, J., Li, C., Higgins, J. P., van de Rijn, M., Bair, E., Montgomery, K., Ferrari, M., Egevad, L., Rayford, W., Bergerheim, U., Ekman, P., DeMarzo, A. M., Tibshirani, R., Botstein, D., Brown, P. O., Brooks, J. D., and Pollack, J. R. (2004) Gene expression profiling identifies clinically relevant subtypes of prostate cancer. *Proc. Natl. Acad. Sci. U.S.A.* **101,** 811–816
17. LaTulippe, E., Satagopan, J., Smith, A., Scher, H., Scardino, P., Reuter, V., and Gerald, W. L. (2002) Comprehensive gene expression analysis of prostate cancer reveals distinct transcriptional programs associated with metastatic disease. *Cancer Res.* **62,** 4499–4506
18. Luo, J., Duggan, D. J., Chen, Y., Sauvageot, J., Ewing, C. M., Bittner, M. L., Trent, J. M., and Isaacs, W. B. (2001) Human prostate cancer and benign prostatic hyperplasia: molecular dissection by gene expression profiling. *Cancer Res.* **61,** 4683–4688
19. Luo, J. H., Yu, Y. P., Cieply, K., Lin, F., Deflavia, P., Dhir, R., Finkelstein, S., Michalopoulos, G., and Becich, M. (2002) Gene expression analysis of prostate cancers. *Mol. Carcinog.* **33,** 25–35
20. Magee, J. A., Araki, T., Patil, S., Ehrig, T., True, L., Humphrey, P. A., Catalona, W. J., Watson, M. A., and Milbrandt, J. (2001) Expression profiling reveals hepsin overexpression in prostate cancer. *Cancer Res.* **61,** 5692–5696
21. Singh, D., Febbo, P. G., Ross, K., Jackson, D. G., Manola, J., Ladd, C., Tamayo, P., Renshaw, A. A., D'Amico, A. V., Richie, J. P., Lander, E. S., Loda, M., Kantoff, P. W., Golub, T. R., and Sellers, W. R. (2002) Gene expression correlates of clinical prostate cancer behavior. *Cancer Cell* **1,** 203–209
22. Welsh, J. B., Sapinoso, L. M., Su, A. I., Kern, S. G., Wang-Rodriguez, J., Moskaluk, C. A., Frierson, H. F., Jr., and Hampton, G. M. (2001) Analysis of gene expression identifies candidate markers and pharmacological targets in prostate cancer. *Cancer Res.* **61,** 5974–5978
23. Yu, Y. P., Landsittel, D., Jing, L., Nelson, J., Ren, B., Liu, L., McDonald, C., Thomas, R., Dhir, R., Finkelstein, S., Michalopoulos, G., Becich, M., and Luo, J. H. (2004) Gene expression alterations in prostate cancer predicting tumor aggression and preceding development of malignancy. *J. Clin. Oncol.* **22,** 2790–2799
24. Golub, T. R., Slonim, D. K., Tamayo, P., Huard, C., Gaasenbeek, M., Mesirov, J. P., Coller, H., Loh, M. L., Downing, J. R., Caligiuri, M. A., Bloomfield, C. D., and Lander, E. S. (1999) Molecular classification of cancer: class discovery and class prediction by gene expression monitoring. *Science* **286,** 531–537
25. Hedenfalk, I., Duggan, D., Chen, Y., Radmacher, M., Bittner, M., Simon, R., Meltzer, P., Gusterson, B., Esteller, M., Kallioniemi, O. P., Wilfond, B., Borg, A., Trent, J., Raffeld, M., Yakhini, Z., Ben-Dor, A., Dougherty, E., Kononen, J., Bubendorf, L., Fehrle, W., Pittaluga, S., Gruvberger, S., Loman, N., Johannsson, O., Olsson, H., and Sauter, G. (2001) Gene-expression profiles in hereditary breast cancer. *N. Engl. J. Med.* **344,** 539–548
26. Perou, C. M., Sørlie, T., Eisen, M. B., van de Rijn, M., Jeffrey, S. S., Rees, C. A., Pollack, J. R., Ross, D. T., Johnsen, H., Akslen, L. A., Fluge, O., Pergamenschikov, A., Williams, C., Zhu, S. X., Lønning, P. E., Børresen-Dale, A. L., Brown, P. O., and Botstein, D. (2000) Molecular portraits of human breast tumours. *Nature* **406,** 747–752
27. Alizadeh, A. A., Eisen, M. B., Davis, R. E., Ma, C., Lossos, I. S., Rosenwald, A., Boldrick, J. C., Sabet, H., Tran, T., Yu, X., Powell, J. I., Yang, L., Marti, G. E., Moore, T., Hudson, J., Jr., Lu, L., Lewis, D. B., Tibshirani, R., Sherlock, G., Chan, W. C., Greiner, T. C., Weisenburger, D. D., Armitage, J. O., Warnke, R., Levy, R., Wilson, W., Grever, M. R., Byrd, J. C., Botstein, D., Brown, P. O., and Staudt, L. M. (2000) Distinct types of diffuse large B-cell lymphoma identified by gene expression profiling. *Nature* **403,** 503–511
28. Nelson, P. S., Han, D., Rochon, Y., Corthals, G. L., Lin, B., Monson, A., Nguyen, V., Franza, B. R., Plymate, S. R., Aebersold, R., and Hood, L. (2000) Comprehensive analyses of prostate gene expression: convergence of expressed sequence tag databases, transcript profiling and proteomics. *Electrophoresis* **21,** 1823–1831
29. Ahram, M., Best, C. J., Flaig, M. J., Gillespie, J. W., Leiva, I. M., Chuaqui, R. F., Zhou, G., Shu, H., Duray, P. H., Linehan, W. M., Raffeld, M., Ornstein, D. K., Zhao, Y., Petricoin, E. F., 3rd, and Emmert-Buck, M. R. (2002) Proteomic analysis of human prostate cancer. *Mol. Carcinog.* **33,** 9–15
30. Sreekumar, A., Laxman, B., Rhodes, D. R., Bhagavathula, S., Harwood, J., Giacherio, D., Ghosh, D., Sanda, M. G., Rubin, M. A., and Chinnaiyan, A. M. (2004) Humoral immune response to alpha-methylacyl-CoA racemase and prostate cancer. *J. Natl. Cancer Inst.* **96,** 834–843
31. Comuzzi, B., and Sadar, M. D. (2006) Proteomic analyses to identify novel therapeutic targets for the treatment of advanced prostate cancer. *Cellscience* **3,** 61–81
32. Garbis, S. D., Tyritzis, S. I., Roumeliotis, T., Zerefos, P., Giannopoulou, E. G., Vlahou, A., Kossida, S., Diaz, J., Vourekas, S., Tamvakopoulos, C., Pavlakis, K., Sanoudou, D., and Constantinides, C. A. (2008) Search for potential markers for prostate cancer diagnosis, prognosis and treatment

in clinical tissue specimens using amine-specific isobaric tagging (iTRAQ) with two-dimensional liquid chromatography and tandem mass spectrometry. *J. Proteome Res.* **7,** 3146–3158
33. Glen, A., Gan, C. S., Hamdy, F. C., Eaton, C. L., Cross, S. S., Catto, J. W., Wright, P. C., and Rehman, I. (2008) iTRAQ-facilitated proteomic analysis of human prostate cancer cells identifies proteins associated with progression. *J. Proteome Res*. **7,** 897–907
34. Matta, A., DeSouza, L. V., Shukla, N. K., Gupta, S. D., Ralhan, R., and Siu, K. W. (2008) Prognostic significance of head-and-neck cancer biomarkers previously discovered and identified using iTRAQ-labeling and multidimensional liquid chromatography-tandem mass spectrometry. *J. Proteome Res.* **7,** 2078–2087
35. Ralhan, R., Desouza, L. V., Matta, A., Chandra Tripathi, S., Ghanny, S., Datta Gupta, S., Bahadur, S., and Siu, K. W. (2008) Discovery and verification of head-and-neck cancer biomarkers by differential protein expression analysis using iTRAQ labeling, multidimensional liquid chromatography, and tandem mass spectrometry. *Mol. Cell. Proteomics* **7,** 1162–1173
36. Keshamouni, V. G., Michailidis, G., Grasso, C. S., Anthwal, S., Strahler, J. R., Walker, A., Arenberg, D. A., Reddy, R. C., Akulapalli, S., Thannickal, V. J., Standiford, T. J., Andrews, P. C., and Omenn, G. S. (2006) Differential protein expression profiling by iTRAQ-2DLC-MS/MS of lung cancer cells undergoing epithelial-mesenchymal transition reveals a migratory/invasive phenotype. *J. Proteome Res.* **5,** 1143–1154
37. Nesvizhskii, A. I., Vitek, O., and Aebersold, R. (2007) Analysis and validation of proteomic data generated by tandem mass spectrometry. *Nat. Methods* **4,** 787–797
38. R Development Core Team (2008) *R: a Language and Environment for Statistical Computing*, R Foundation for Statistical Computing, Vienna
39. Rhodes, D. R., Kalyana-Sundaram, S., Tomlins, S. A., Mahavisno, V., Kasper, N., Varambally, R., Barrette, T. R., Ghosh, D., Varambally, S., and Chinnaiyan, A. M. (2007) Molecular concepts analysis links tumors, pathways, mechanisms, and drugs. *Neoplasia* **9,** 443–454
40. Tomlins, S. A., Mehra, R., Rhodes, D. R., Cao, X., Wang, L., Dhanasekaran, S. M., Kalyana-Sundaram, S., Wei, J. T., Rubin, M. A., Pienta, K. J., Shah, R. B., and Chinnaiyan, A. M. (2007) Integrative molecular concept modeling of prostate cancer progression. *Nat. Genet.* **39,** 41–51
41. Taylor, B. S., Pal, M., Yu, J., Laxman, B., Kalyana-Sundaram, S., Zhao, R., Menon, A., Wei, J. T., Nesvizhskii, A. I., Ghosh, D., Omenn, G. S., Lubman, D. M., Chinnaiyan, A. M., and Sreekumar, A. (2008) Humoral response profiling reveals pathways to prostate cancer progression. *Mol. Cell. Proteomics* **7,** 600–611
42. Yu, J., Cao, Q., Mehra, R., Laxman, B., Yu, J., Tomlins, S. A., Creighton, C. J., Dhanasekaran, S. M., Shen, R., Chen, G., Morris, D. S., Marquez, V. E., Shah, R. B., Ghosh, D., Varambally, S., and Chinnaiyan, A. M. (2007) Integrative genomics analysis reveals silencing of beta-adrenergic signaling by polycomb in prostate cancer. *Cancer Cell* **12,** 419–431
43. Yu, J., Yu, J., Rhodes, D. R., Tomlins, S. A., Cao, X., Chen, G., Mehra, R., Wang, X., Ghosh, D., Shah, R. B., Varambally, S., Pienta, K. J., and Chinnaiyan, A. M. (2007) A polycomb repression signature in metastatic prostate cancer predicts cancer outcome. *Cancer Res.* **67,** 10657–10663
44. Krützfeldt, J., Rajewsky, N., Braich, R., Rajeev, K. G., Tuschl, T., Manoharan, M., and Stoffel, M. (2005) Silencing of microRNAs in vivo with 'antagomirs'. *Nature* **438,** 685–689
45. Varambally, S., Laxman, B., Mehra, R., Cao, Q., Dhanasekaran, S. M., Tomlins, S. A., Granger, J., Vellaichamy, A., Sreekumar, A., Yu, J., Gu, W., Shen, R., Ghosh, D., Wright, L. M., Kladney, R. D., Kuefer, R., Rubin, M. A., Fimmel, C. J., and Chinnaiyan, A. M. (2008) Golgi protein GOLM1 is a tissue and urine biomarker of prostate cancer. *Neoplasia* **10,** 1285–1294
46. Jalava, S. E., Porkka, K. P., Rauhala, H. E., Isotalo, J., Tammela, T. L., and Visakorpi, T. (2009) TCEB1 promotes invasion of prostate cancer cells. *Int. J. Cancer* **124,** 95–102
47. Ruscica, M., Dozio, E., Motta, M., and Magni, P. (2007) Modulatory actions of neuropeptide Y on prostate cancer growth: role of MAP kinase/ERK 1/2 activation. *Adv. Exp. Med. Biol*. **604,** 96–100
48. Hod, Y. (2004) Differential control of apoptosis by DJ-1 in prostate benign and cancer cells. *J. Cell. Biochem.* **92,** 1221–1233
49. Zhang, Y., Forootan, S. S., Liu, D., Barraclough, R., Foster, C. S., Rudland, P. S., and Ke, Y. (2007) Increased expression of anterior gradient-2 is significantly associated with poor survival of prostate cancer patients. *Prostate Cancer Prostatic Dis.* **10,** 293–300
50. Hood, B. L., Darfler, M. M., Guiel, T. G., Furusato, B., Lucas, D. A., Ringeisen, B. R., Sesterhenn, I. A., Conrads, T. P., Veenstra, T. D., and Krizman, D. B. (2005) Proteomic analysis of formalin-fixed prostate cancer tissue. *Mol. Cell. Proteomics* **4,** 1741–1753
51. Grzmil, M., Voigt, S., Thelen, P., Hemmerlein, B., Helmke, K., and Burfeind, P. (2004) Up-regulated expression of the MAT-8 gene in prostate cancer and its siRNA-mediated inhibition of expression induces a decrease in proliferation of human prostate carcinoma cells. *Int. J. Oncol*. **24,** 97–105
52. Korkmaz, C. G., Korkmaz, K. S., Kurys, P., Elbi, C., Wang, L., Klokk, T. I., Hammarstrom, C., Troen, G., Svindland, A., Hager, G. L., and Saatcioglu, F. (2005) Molecular cloning and characterization of STAMP2, an androgen-regulated six transmembrane protein that is overexpressed in prostate cancer. *Oncogene* **24,** 4934–4945
53. Adamson, J., Morgan, E. A., Beesley, C., Mei, Y., Foster, C. S., Fujii, H., Rudland, P. S., Smith, P. H., and Ke, Y. (2003) High-level expression of cutaneous fatty acid-binding protein in prostatic carcinomas and its effect on tumorigenicity. *Oncogene* **22,** 2739–2749
54. Wu, M., Bai, X., Xu, G., Wei, J., Zhu, T., Zhang, Y., Li, Q., Liu, P., Song, A., Zhao, L., Gang, C., Han, Z., Wang, S., Zhou, J., Lu, Y., and Ma, D. (2007) Proteome analysis of human androgen-independent prostate cancer cell lines: variable metastatic potentials correlated with vimentin expression. *Proteomics* **7,** 1973–1983
55. Shaheduzzaman, S., Vishwanath, A., Furusato, B., Cullen, J., Chen, Y., Bañez, L., Nau, M., Ravindranath, L., Kim, K. H., Mohammed, A., Chen, Y., Ehrich, M., Srikantan, V., Sesterhenn, I. A., McLeod, D., Vahey, M., Petrovics, G., Dobi, A., and Srivastava, S. (2007) Silencing of lactotransferrin expression by methylation in prostate cancer progression. *Cancer Biol. Ther.* **6,** 1088–1095
56. Henshall, S. M., Horvath, L. G., Quinn, D. I., Eggleton, S. A., Grygiel, J. J., Stricker, P. D., Biankin, A. V., Kench, J. G., and Sutherland, R. L. (2006) Zinc-alpha2-glycoprotein expression as a predictor of metastatic prostate cancer following radical prostatectomy. *J. Natl. Cancer Inst.* **98,** 1420–1424
57. Beke, L., Nuytten, M., Van Eynde, A., Beullens, M., and Bollen, M. (2007) The gene encoding the prostatic tumor suppressor PSP94 is a target for repression by the Polycomb group protein EZH2. *Oncogene* **26,** 4590–4595
58. Medeiros, R., Vasconcelos, A., Costa, S., Pinto, D., Ferreira, P., Lobo, F., Morais, A., Oliveira, J., and Lopes, C. (2004) Metabolic susceptibility genes and prostate cancer risk in a southern European population: the role of glutathione S-transferases GSTM1, GSTM3, and GSTT1 genetic polymorphisms. *Prostate* **58,** 414–420
59. Bostwick, D. G., Meiers, I., and Shanks, J. H. (2007) Glutathione S-transferase: differential expression of alpha, mu, and pi isoenzymes in benign prostate, prostatic intraepithelial neoplasia, and prostatic adenocarcinoma. *Hum. Pathol.* **38,** 1394–1401
60. Meiers, I., Shanks, J. H., and Bostwick, D. G. (2007) Glutathione S-transferase pi (GSTP1) hypermethylation in prostate cancer: review 2007. *Pathology* **39,** 299–304
61. Leiblich, A., Cross, S. S., Catto, J. W., Phillips, J. T., Leung, H. Y., Hamdy, F. C., and Rehman, I. (2006) Lactate dehydrogenase-B is silenced by promoter hypermethylation in human prostate cancer. *Oncogene* **25,** 2953–2960
62. Segawa, T., Nau, M. E., Xu, L. L., Chilukuri, R. N., Makarem, M., Zhang, W., Petrovics, G., Sesterhenn, I. A., McLeod, D. G., Moul, J. W., Vahey, M., and Srivastava, S. (2002) Androgen-induced expression of endoplasmic reticulum (ER) stress response genes in prostate cancer cells. *Oncogene* **21,** 8749–8758
63. Wang, J., Wang, J., Dai, J., Jung, Y., Wei, C. L., Wang, Y., Havens, A. M., Hogg, P. J., Keller, E. T., Pienta, K. J., Nor, J. E., Wang, C. Y., and Taichman, R. S. (2007) A glycolytic mechanism regulating an angiogenic switch in prostate cancer. *Cancer Res.* **67,** 149–159
64. He, X. Y., Yang, Y. Z., Peehl, D. M., Lauderdale, A., Schulz, H., and Yang, S. Y. (2003) Oxidative 3alpha-hydroxysteroid dehydrogenase activity of human type 10 17beta-hydroxysteroid dehydrogenase. *J. Steroid Biochem. Mol. Biol.* **87,** 191–198
65. Ghosh, A. K., Steele, R., and Ray, R. B. (2005) c-myc Promoter-binding protein 1 (MBP-1) regulates prostate cancer cell growth by inhibiting MAPK pathway. *J. Biol. Chem.* **280,** 14325–14330
66. Locke, J. A., Wasan, K. M., Nelson, C. C., Guns, E. S., and Leon, C. G.

ASBMB MOLECULAR & CELLULAR PROTEOMICS MCP

(2008) Androgen-mediated cholesterol metabolism in LNCaP and PC-3 cell lines is regulated through two different isoforms of acyl-coenzyme A:cholesterol acyltransferase (ACAT). *Prostate* **68,** 20–33
67. Weber, A., Kristiansen, I., Johannsen, M., Oelrich, B., Scholmann, K., Gunia, S., May, M., Meyer, H. A., Behnke, S., Moch, H., and Kristiansen, G. (2008) The FUSE binding proteins FBP1 and FBP3 are potential c-myc regulators in renal, but not in prostate and bladder cancer. *BMC Cancer* **8,** 369
68. Saal, L. H., Johansson, P., Holm, K., Gruvberger-Saal, S. K., She, Q. B., Maurer, M., Koujak, S., Ferrando, A. A., Malmström, P., Memeo, L., Isola, J., Bendahl, P. O., Rosen, N., Hibshoosh, H., Ringnér, M., Borg, A., and Parsons, R. (2007) Poor prognosis in carcinoma is associated with a gene expression signature of aberrant PTEN tumor suppressor pathway activity. *Proc. Natl. Acad. Sci. U.S.A.* **104,** 7564–7569
69. Harada, N., Ohmori, Y., Yamaji, R., Higashimura, Y., Okamoto, K., Isohashi, F., Nakano, Y., and Inui, H. (2008) ARA24/Ran enhances the androgen-dependent NH2- and COOH-terminal interaction of the androgen receptor. *Biochem. Biophys. Res. Commun.* **373,** 373–377
70. Cross, S. S., Hamdy, F. C., Deloulme, J. C., and Rehman, I. (2005) Expression of S100 proteins in normal human tissues and common cancers using tissue microarrays: S100A6, S100A8, S100A9 and S100A11 are all overexpressed in common cancers. *Histopathology* **46,** 256–269
71. Bostwick, D. G., Alexander, E. E., Singh, R., Shan, A., Qian, J., Santella, R. M., Oberley, L. W., Yan, T., Zhong, W., Jiang, X., and Oberley, T. D. (2000) Antioxidant enzyme expression and reactive oxygen species damage in prostatic intraepithelial neoplasia and cancer. *Cancer* **89,** 123–134
72. Niu, Y., Altuwaijri, S., Lai, K. P., Wu, C. T., Ricke, W. A., Messing, E. M., Yao, J., Yeh, S., and Chang, C. (2008) Androgen receptor is a tumor suppressor and proliferator in prostate cancer. *Proc. Natl. Acad. Sci. U.S.A.* **105,** 12182–12187
73. Papadopoulou, N., Charalampopoulos, I., Alevizopoulos, K., Gravanis, A., and Stournaras, C. (2008) Rho/ROCK/actin signaling regulates membrane androgen receptor induced apoptosis in prostate cancer cells. *Exp. Cell Res.* **314,** 3162–3174
74. Nishimura, K., Ting, H. J., Harada, Y., Tokizane, T., Nonomura, N., Kang, H. Y., Chang, H. C., Yeh, S., Miyamoto, H., Shin, M., Aozasa, K., Okuyama, A., and Chang, C. (2003) Modulation of androgen receptor transactivation by gelsolin: a newly identified androgen receptor coregulator. *Cancer Res.* **63,** 4888–4894
75. Ellerhorst, J., Troncoso, P., Xu, X. C., Lee, J., and Lotan, R. (1999) Galectin-1 and galectin-3 expression in human prostate tissue and prostate cancer. *Urol. Res.* **27,** 362–367
76. Lowery, A. J., Miller, N., McNeill, R. E., and Kerin, M. J. (2008) MicroRNAs as prognostic indicators and therapeutic targets: potential effect on breast cancer management. *Clin. Cancer Res.* **14,** 360–365
77. Kleer, C. G., Cao, Q., Varambally, S., Shen, R., Ota, I., Tomlins, S. A., Ghosh, D., Sewalt, R. G., Otte, A. P., Hayes, D. F., Sabel, M. S., Livant, D., Weiss, S. J., Rubin, M. A., and Chinnaiyan, A. M. (2003) EZH2 is a marker of aggressive breast cancer and promotes neoplastic transformation of breast epithelial cells. *Proc. Natl. Acad. Sci. U.S.A.* **100,** 11606–11611
78. Zhang, Y., Chao, T., Li, R., Liu, W., Chen, Y., Yan, X., Gong, Y., Yin, B., Liu, W., Qiang, B., Zhao, J., Yuan, J., and Peng, X. (2009) MicroRNA-128 inhibits glioma cells proliferation by targeting transcription factor E2F3a. *J. Mol. Med*. **87,** 43–51
79. Kochevar, G. J., Brody, J. R., Kadkol, S. S., Murphy, K. M., and Pasternack, G. R. (2004) Identification of a functional mutation in pp32r1 (ANP32C). *Hum. Mutat.* **23,** 546–551
80. Shi, J., Hu, Z., Pabon, K., and Scotto, K. W. (2008) Caffeine regulates alternative splicing in a subset of cancer-associated genes: a role for SC35. *Mol. Cell. Biol.* **28,** 883–895
81. Lee, C. F., Ling, Z. Q., Zhao, T., Fang, S. H., Chang, W. C., Lee, S. C., and Lee, K. R. (2009) Genomic-wide analysis of lymphatic metastasis-associated genes in human hepatocellular carcinoma. *World J. Gastroenterol.* **15,** 356–365
82. Alcalá, S., Klee, M., Fernández, J., Fleischer, A., and Pimentel-Muiños, F. X. (2008) A high-throughput screening for mammalian cell death effectors identifies the mitochondrial phosphate carrier as a regulator of cytochrome c release. *Oncogene.* **27,** 44–54
83. Sreekumar, A., Poisson, L. M., Rajendiran, T. M., Khan, A. P., Cao, Q., Yu, J., Laxman, B., Mehra, R., Lonigro, R. J., Li, Y., Nyati, M. K., Ahsan, A., Kalyana-Sundaram, S., Han, B., Cao, X., Byun, J., Omenn, G. S., Ghosh, D., Pennathur, S., Alexander, D. C., Berger, A., Shuster, J. R., Wei, J. T., Varambally, S., Beecher, C., and Chinnaiyan, A. M. (2009) Metabolomic profiles delineate potential role for sarcosine in prostate cancer progression. *Nature* **457,** 910–914
84. Varambally, S., Cao, Q., Mani, R. S., Shankar, S., Wang, X., Ateeq, B., Laxman, B., Cao, X., Jing, X., Ramnarayanan, K., Brenner, J. C., Yu, J., Kim, J. H., Han, B., Tan, P., Kumar-Sinha, C., Lonigro, R. J., Palanisamy, N., Maher, C. A., and Chinnaiyan, A. M. (2008) Genomic loss of microRNA-101 leads to overexpression of histone methyltransferase EZH2 in cancer. *Science* **322,** 1695–1699
85. Evangelisti, C., Florian, M. C., Massimi, I., Dominici, C., Giannini, G., Galardi, S., Buè, M. C., Massalini, S., McDowell, H. P., Messi, E., Gulino, A., Farace, M. G., and Ciafrè, S. A. (2009) MiR-128 up-regulation inhibits Reelin and DCX expression and reduces neuroblastoma cell motility and invasiveness. *FASEB J.* **23,** 4276–4287

ASBMB MOLECULAR & CELLULAR PROTEOMICS MCP